A Section 508–conformant HTML version of this article is available at https://doi.org/10.1289/EHP10923.

Prolonged, Low-Level Exposure to the Marine Toxin, Domoic Acid, and Measures of Neurotoxicity in Nonhuman Primates

Rebekah L. Petroff,[1] Christopher Williams,[2] Jian-Liang Li,[3] James W. MacDonald,[1] Theo K. Bammler,[1] Todd Richards,[4] Christopher N. English,[5] Audrey Baldessari,[5] Sara Shum,[6] Jing Jing,[6] Nina Isoherranen,[6,7] Brenda Crouthamel,[1] Noelle McKain,[1] Kimberly S. Grant,[1,5] Thomas M. Burbacher,[1,5,7] and G. Jean Harry[2]*

[1]Department of Environmental and Occupational Health Sciences, University of Washington, Seattle, Washington, USA
[2]Mechanistic Toxicology Branch, Division of the National Toxicology Program, National Institute of Environmental Health Sciences (NIEHS), National Institutes of Health (NIH), Department of Health and Human Services (DHHS), Research Triangle Park, North Carolina, USA
[3]Epigenetics & Stem Cell Biology Laboratory, NIEHS, NIH, DHHS, Research Triangle Park, North Carolina, USA
[4]Department of Radiology, University of Washington, Seattle, Washington, USA
[5]Washington National Primate Research Center, Seattle, Washington, USA
[6]Department of Pharmaceutics, University of Washington, Seattle, Washington, USA
[7]Center on Human Development and Disability, University of Washington, Seattle, Washington, USA

Background: The excitotoxic molecule, domoic acid (DA), is a marine algal toxin known to induce overt hippocampal neurotoxicity. Recent experimental and epidemiological studies suggest adverse neurological effects at exposure levels near the current regulatory limit (20 ppm, ~0.075–0.1 mg/kg). At these levels, cognitive effects occur in the absence of acute symptoms or evidence of neuronal death.

Objectives: This study aimed to identify adverse effects on the nervous system from prolonged, dietary DA exposure in adult, female *Macaca fascicularis* monkeys.

Methods: Monkeys were orally exposed to 0, 0.075, and 0.15 mg/kg per day for an average of 14 months. Clinical blood counts, chemistry, and cytokine levels were analyzed in the blood. In-life magnetic resonance (MR) imaging assessed volumetric and tractography differences in and between the hippocampus and thalamus. Histology of neurons and glia in the fornix, fimbria, internal capsule, thalamus, and hippocampus was evaluated. Hippocampal RNA sequencing was used to identify differentially expressed genes. Enrichment of gene networks for neuronal health, excitotoxicity, inflammation/glia, and myelin were assessed with Gene Set Enrichment Analysis.

Results: Clinical blood counts, chemistry, and cytokine levels were not altered with DA exposure in nonhuman primates. Transcriptome analysis of the hippocampus yielded 748 differentially expressed genes (fold change ≥ 1.5; $p \leq 0.05$), reflecting differences in a broad molecular profile of intermediate early genes (e.g., *FOS, EGR*) and genes related to myelin networks in DA animals. Between exposed and control animals, MR imaging showed comparable connectivity of the hippocampus and thalamus and histology showed no evidence of hypomyelination. Histological examination of the thalamus showed a larger microglia soma size and an extension of cell processes, but suggestions of a $GFAP^{+}$astrocyte response showed no indication of astrocyte hypertrophy.

Discussion: In the absence of overt hippocampal excitotoxicity, chronic exposure of *Macaca fascicularis* monkeys to environmentally relevant levels of DA suggested a subtle shift in the molecular profile of the hippocampus and the microglia phenotype in the thalamus that was possibly reflective of an adaptive response due to prolonged DA exposure. https://doi.org/10.1289/EHP10923

Introduction

Domoic acid (DA) is a common marine algal toxin produced by some species of *Pseudo nitzschia*[1,2] and other marine macroalgae, such as *Chondria armata*.[3,4] When present in the water, DA can contaminate shellfish and other types of seafood, including razor clams, scallops, oysters, mussels, anchovies, sardines, and crabs.[5] Consumption of contaminated shellfish can induce neurotoxicity in humans and in a variety of wildlife species, including sea lions,[6] whales, sea otters, and sea birds.[7] The only known acute DA poisoning event in humans occurred in 1987 when the consumption of blue mussels (*Mytilus edulis*), contaminated with ~70 mg DA/100 g of tissue weight, resulted in >200 cases of illness.[8] Of these, 107 patients had confirmed cases of a severe neurotoxic syndrome, later named amnesic shellfish poisoning (ASP), with an estimated exposure of ~270–290 mg of DA per person. Clinical presentation of ASP was characterized by gastrointestinal symptoms (gastrointestinal distress, vomiting, diarrhea) within 24 h of consumption and accompanying neurological symptoms within 48 h. Neurological symptoms were wide ranging and included headache, coma, seizures, and memory loss, harkening to the "amnesic" label of ASP.[9]

In a follow-up of 14 patients with pronounced neurological dysfunction, the initial response to DA poisoning occurred between 4 and 72 h postexposure, with a general recovery within 24 h to 12 wk.[10] In patients with prolonged memory loss, brain imaging revealed reduced glucose metabolism in the hippocampus and medial temporal lobe.[10] Although a long-term follow-up of these patients was not formally conducted, 1 patient with an initial severe case of ASP presented 1 y later with complex partial seizures involving clonic movements of the arm and leg that were accompanied by severe memory impairment.[11] Imaging in this patient revealed marked atrophy in the hippocampus; this pattern of neurodegeneration was supported by posthumous histological examination. This detailed symptomology and neuropathology that has been previously observed in humans with acute poisonings has also been observed in wildlife[12–14] and experimental animal models.[15–18]

To protect people from severe, excitotoxic neurological effects, the U.S. Food and Drug Administration established an action level of 20 ppm of DA in shellfish tissue.[19] The regulatory limit is equivalent to ~0.075–0.1 mg/kg body weight (BW) per day and is set to protect people from acutely toxic exposures.[20–23] However, concerns for the health effects due to prolonged low-level exposure

Address correspondence to Rebekah L. Petroff, 1415 Washington Heights, Ann Arbor, MI 48109 USA. Email: petrofrl@umich.edu
*Current Affiliation: Department of Environmental Health Sciences, University of Michigan, Ann Arbor, MI

Supplemental Material is available online (https://doi.org/10.1289/EHP10923).
The authors declare they have nothing to disclose.
Received 10 January 2022; Revised 21 July 2022; Accepted 9 August 2022; Published 14 September 2022.

have been raised by recent epidemiological studies, which have suggested an association between memory deficits and repeated dietary exposure to DA at levels below the regulatory limit.[24–27] Specific populations that are of highest risk of this type of exposure are both coastal subsistence shellfish harvesters[28] and consumers in Native American communities[29] who are economically and culturally reliant on defined food sources. A more recent concern has also been raised for populations who are in situations of increasingly repeated intermittent exposures as a result of global climate shifts in the occurrence of algal blooms.[30,31]

With the hippocampal excitotoxicity induced by acute DA exposure, various injury-induced responses associated with neuronal damage have also been reported, including astrocyte and microglia reactions.[32,33] Experimental rodent studies examining the neurotoxic effects of low-level DA exposure have reported subtle effects on the nervous system in the absence of typical DA excitotoxicity.[34,35] It is thought that at these lower exposures, DA may act as a glutamate agonist, altering normal neuronal and synaptic function and promoting inflammatory responses in the absence of overt neuronal death. In mice, a prolonged, low-level DA exposure resulted in spatial memory deficits in the absence of hippocampal neuropathology.[36] Subtle differences were, however, observed in vesicular glutamate transporter 1 (VGluT1) expression within hippocampal cornu ammonis area (CA) 1 excitatory boutons, representing a possible alteration of glutamatergic transmission in CA1 that was linked with the disruption of spatial memory.[37] In adult nonhuman primates, it was not thought that these lower exposures resulted in toxic effects[38] until recently.[39] In a translational study designed to capture the structural and functional similarity between monkey and human brains,[40,41] as well as the similarities with contemporary human exposures to DA,[26,28,42] exposed monkeys had tremors and targeted effects on myelination from whole-brain magnetic resonance (MR) imaging.[43] Although MR imaging can be an effective translational tool in describing and identifying neurotoxic injury,[44] paired histopathological and MR imaging studies can have discordant findings, especially at lower resolution.[45,46] Thus, subsequent studies employing immunohistochemical assessments and targeted MR imaging analysis can help validate findings or offer alternative explanations. Given the growing concerns from low-level DA exposure scenarios, detailed studies of cellular responses in a model closely related to humans, and with an oral exposure paradigm, could help identify the potential neurotoxic mechanisms of low-level exposure to DA.

The present study assessed the cellular-level effects after prolonged, oral exposure to low levels of DA in a nonhuman primate model by expanding on previous assessments in a cohort of female *Macaca fascicularis* monkeys exposed to DA, daily, for an average of 14 months (at 0.075 or 0.15 mg/kg BW per day).[39] These oral exposures were selected to closely resemble both the maximum allowable regulatory limit (20 ppm in shellfish meat, which was estimated to be 0.075–0.1 mg/kg for an average adult)[20–23] and contemporary exposures based on the consumption of contaminated razor clams in Washington State (0.003–0.09 mg/kg BW per day, depending on DA concentrations in shellfish).[28] As previously reported in this cohort of monkeys, daily DA exposure did not result in altered BWs or induce alterations in general observational clinical health assessment, but tremors were reported after as little as 2 months of DA exposure.[39] In-life, whole-brain MR imaging of these animals showed no evidence of overt damage or disorganization; however, lower brain-wide fractional anisotropy (FA) was correlated with tremors.[43] These specific differences were suggestive of a subtle alteration in white matter integrity in the fornix, internal capsule, brainstem, and corpus callosum.[43] Using this same cohort of animals, the present study used region-specific MR imaging techniques, histological assessments, and RNA sequencing (RNAseq) to assess DA-related evidence of hippocampal excitotoxicity or neuronal death, differences in myelination, and responses of astrocytes and microglia.

Methods

Animals

Adult female *Macaca fascicularis* monkeys between 5.5 and 11 years of age (average = 6.9 y) and 2.8–4.2 kg in BW (average = 3.6 kg) were originally obtained from Charles River Laboratory, Alpha Genesis Incorporated, and Valley Biosystems (Table S1). Animals were housed in the Infant Primate Research Laboratory at the Washington National Primate Research Center in Seattle, Washington, USA. Females were individually housed with grooming bars that allowed contact and communication with an adjacent female social partner, 24 h/d. Environmental enrichment (e.g., frozen treats, fresh fruit and vegetables, music, puzzle toys) was provided daily. The room was maintained at 24 ± 4°C on a 12-h light/dark schedule. Animals were provided High Protein Monkey Diet biscuits (Lab Diet) twice a day and filtered drinking water *ad libitum*. All research protocols adhered to the guidance of the Animal Welfare Act[47] and the *Guide for Care and Use of Laboratory Animals* from the National Research Council[48] and were approved by the University of Washington Institutional Animal Care and Use Committee.

Study Periods

The study represents five key periods: Baseline (2 months, where training occurred); Initial Dosing (2 months); Breeding (1–7 months, average = 2.7 months, dependent on how many timed cycles until pregnancy); Pregnancy (6 months); and Postpartum (1–8 months, average = 6.3 months). Animals underwent necropsy at the end of the Postpartum period (8–23 months, average = 14.0 months). A schematic of the timeline of exposure and assessments is provided in Figure 1. Previously reported results of this cohort have been published in several articles already, including ones detailing pharmacokinetic outcomes in the Initial Dosing and Pregnancy periods,[49–51] reproductive outcomes in the Breeding and Pregnancy periods,[39] whole-brain MR imaging in the Postpartum period,[43] and electrophysiology in the Postpartum period.[52] The present article describes the continued investigation of an unexpected clinical sign of neurotoxicity (tremor) that was associated with chronic DA exposure.[39]

All investigator interactions with the animals were conducted under coded conditions to maintain experimental blinding across the study. During Baseline, standard positive reinforcement techniques were used to train animals to drink 1 mL of solution from a 3-mL syringe without restraint to facilitate oral dosing of DA in the study. Animals were acclimated to aspects of the study: weekly weighing; a series of tasks designed to assess clinical toxicity; and unsedated, intravenous (IV) blood draws from the saphenous vein in a procedure cage attached to their home cage. All acclimation procedures were conducted prior to DA exposure.

DA Exposure

DA was purchased from BioVectra. Certified calibration solution for DA was purchased from National Research Council Canada. Individual dosing solutions were prepared weekly, according to animal weight and dose group, in a filtered, 5% sucrose solution in water and stored in 16-mL glass vials at 4°C until use. Each solution was prepared with sonication for 15 min. Concentrations of DA doses were confirmed by high-performance liquid chromatography with tandem mass spectrometry (HPLC-MS/MS).[49,50] In brief, samples were measured using an AB Sciex 5500 qTrap Q-LIT mass spectrometer (AB Sciex), equipped with an Agilent 1290 ultra-HPLC

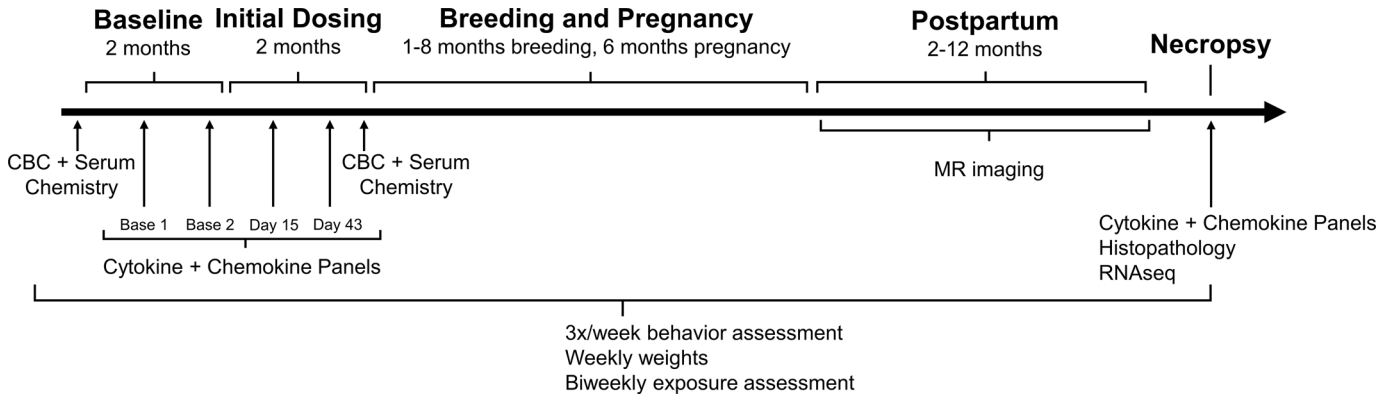

Figure 1. Timeline of study. Representation of the five stages of the study: Baseline (prior to dosing), Initial Dosing (~2 months prior to breeding), Breeding and Pregnancy, Postpartum. Necropsy occurred in the Postpartum period. Daily, oral domoic acid (DA) dosing began in the Initial Dosing period and continued through Breeding and Pregnancy. A subset of animals was continued on daily dosing in the Postpartum period (see Table S1 for details). Blood samples for complete blood counts (CBCs) and serum chemistry were collected at the beginning of study (Baseline) and at the end of the Initial Dosing period (average: day 73). Blood levels of cytokines and chemokines were analyzed twice during Baseline, twice during Initial Dosing (average: day 15, day 43), and at necropsy (average: month 14 or 425 d). Magnetic resonance (MR) imaging was conducted during the Postpartum period. Tissue was collected at necropsy for histological assessment and RNA sequencing (RNAseq). Body weights, behavioral assessments, and DA exposure assessments were collected throughout the entire study.

(Agilent Technologies) and a Synergi Hydro-RP 100-Å liquid chromatography column (2.5 mm, 50 × 2 mm; Phenomenex). Samples were placed in the 4°C autosampler and 10 µL of sample was injected for analysis. Gradient elution, 95% for 1 min to 0% over 3 min and then to 95% for 3 min, with a flow rate of 0.5 mL/min, was conducted using water with 0.1% formic acid (A) and using 95% acetonitrile with 5% water and 0.1% formic acid (B). Analytes were detected using positive ion electrospray ionization mode. MS/MS transition for DA was *m/z* 312.2 > 266. All reagents (optima grade water, methanol, acetonitrile, and formic acid) were purchased from Thermo Fisher Scientific.

Adult females were pseudo-randomly assigned to either the control, 0.075, or 0.15-mg/kg BW per day group, controlling for differences in weight and age. Dose groups were maintained across social partners. Animals received daily, oral doses of a 1-mL solution of either 5% sucrose vehicle ($n = 10$), 0.075 mg DA/kg BW ($n = 11$), or 0.15 mg DA/kg BW ($n = 11$) at ~0900 hours, 7 d/wk. Food biscuits were provided at ~2 h before and 5 h after DA exposure.

During the Initial Dosing period, one control animal and one animal in the 0.075-mg/kg BW per day group were excluded from the study because of health conditions unrelated to exposure. This resulted in a total sample size of 30 ($n = 9$ controls; $n = 10$ 0.075-mg/kg BW per day animals; $n = 11$ 0.15-mg/kg BW per day animals). Daily, oral exposures of the females continued during the Breeding period, when females underwent timed-breeding with males not exposed to DA. Twenty-eight females successfully conceived and carried a full-term pregnancy (Table S1). Dosing during pregnancy was based on the individual animal's last prepregnancy BW. Originally, the study was designed to have exposure cease on partition; however, upon the observation of tremor in 3 animals in the 0.075-mg/kg BW per day group and 4 animals in the 0.15-mg/kg BW per day group (who had exposure cease at partition),[39] the remaining females were maintained on DA exposure until necropsy. The 2 animals (A15248, control; A16107, 0.075-mg/kg BW per day group) who did not conceive remained in the study, were maintained on dose, and included in end point assessment where noted (Table S1).

Blood Levels of DA

Blood was collected via restrained, unsedated blood draws from the great saphenous vein, biweekly at 24 h postexposure. A 2-mL volume was collected into 4-mL sodium heparin vacutainer collection tubes (Greiner Bio-One). After collection, blood was centrifuged at 3,000 × *g* for 15 min to isolate plasma and then stored at −20°C until analysis. DA was measured via HPLC-MS/MS methods similar to those outlined above but optimized for nonhuman primate plasma.[49,50] In nonhuman primate plasma, the lower limit of quantification was 0.31 ng/mL and the limit of detection (LOD) was 0.16 ng/mL. Any measure that was detected but below the limit of quantification was imputed with 0.24 ng/mL (halfway between the limit of quantification and LOD). Prior to the Pregnancy period, average blood levels were 0.93 ng/mL (range: 0.24–2.36 ng/mL) and 2.93 ng/mL (range: 0.24–5.26 ng/mL) for the 0.075- and 0.15-mg/kg BW per day DA exposure groups, respectively, and were similar during pregnancy.[39]

Clinical Monitoring

Throughout the study, general health was monitored daily by veterinary clinical staff and BWs were recorded weekly.[39] Clinical exams were conducted by experimentally blinded, trained personnel three times a week, ~5 h after dosing, to evaluate visual functioning and motor coordination. The observational tests were adapted from previously developed clinical observation tests[53,54] and designed to detect behavioral changes in nonhuman primates. Animals were scored using a rating scale on reactivity toward the human tester [neutral, in front or middle of homecage (1); neutral, in back of cage (2); fear grimace (3); threat face (4); displays of aggression (5)] and visual orientation and tracking of a small treat [odd numbers represent right direction; even numbers represent left direction: full track (1 or 2); partial track (3 or 4); orient, but does not track (5 or 6); does not orient (7 or 8)]; and reaching and grabbing the treat [full reach to treat (1); partial reach to treat (2); no reach, but still takes treat from tester (3); will not reach or take treat from tester (4)]. The presence of tremors of the hand or arm during the reach were scored as either absent (0) or present (1).

Complete Blood Counts and Serum Chemistry

To generally monitor health, blood was collected twice for complete blood counts (CBCs) and serum clinical chemistry via restrained, unsedated blood draws from the great saphenous vein: once at the beginning of the Baseline and once at the end of the

Initial Dosing period (at 10 wk of exposure, prior to pregnancy). For CBCs, 4 mL of blood was drawn from the great saphenous vein into ethylenediaminetetraacetic acid (EDTA) microtainer tubes (Greiner Bio-One). For chemistry, 4 mL was drawn into preservative-free serum microtainer tubes (Greiner Bio-One). Samples were immediately transported to the University of Washington Medical Center's Laboratory Medicine facility for processing and analysis.

CBC measures of white blood cell (WBC) count, red blood cell (RBC) count and percentage nucleated RBCs, platelet count, hemoglobin, hematocrit, and counts for neutrophils, lymphocytes, monocytes, eosinophils, and basophils were determined using a Sysmex XN-10 analyzer (Sysmex America, Inc.) according to established human clinical protocols. Cell counts were obtained using impedance technology, enhanced by a sheathed stream with hydrodynamic focused in the RBC/platelet channel and with floating thresholds in the WBC channel to accurately discriminate cell population. Hemoglobin was measured with the sodium lauryl sulfate (SLS) reagent and measured photometrically at 555 nm. One animal in each of the control and the 0.15-mg/kg BW per day groups had a clotted sample that could not be processed (Table S1).

Concentrations of chemistry analytes [sodium, potassium, chloride, blood urea nitrogen, total protein, albumin, globulin, bilirubin, calcium, phosphate, cholesterol, alkaline phosphatase, alanine transaminase (ALT), aspartate aminotransferase (AST), and gamma-glutamyl transferase (GGT)] were determined using a Beckman AU 680/5,812 system (Beckman Coulter, Inc.), following the manufacturer's protocols (see the section "Serum Chemistry Reactions on the Beckman Coulter AU System" in the Supplemental Material).

Cytokine and Chemokine Panels

To assess systemic pro-inflammatory status following DA exposure, inflammatory cytokine and chemokine levels in the blood were determined in nine DA-exposed animals showing evidence of tremor (0.075-mg/kg BW per day group, $n=3$; 0.15-mg/kg BW per day group, $n=6$); and controls, $n=7$ (Table S1). A 4-mL sample of blood was collected from the great saphenous vein in a restrained, unsedated blood draw into sodium heparin vacutainer tubes (Greiner Bio-One) twice prior to DA exposure, once each at 2 and 6 wk of DA exposure (prior to pregnancy), and once at necropsy (post-pregnancy). Samples were rocked by hand and immediately transported to the Interdisciplinary Center for Exposures, Diseases, Genomics and Environment (EDGE) laboratory at the University of Washington. Plasma was separated and stored in 2-mL cryostat tubes at −80°C until analysis.

The V-PLEX NonHuman Primate (NHP) Cytokine 24-Plex Kit from Meso Scale Discovery (Meso Scale Discovery; Catalog# K15058D) was used to determine levels of eotaxin-3, granulocyte–macrophage colony-stimulating factor (GM-CSF), interferon gamma (IFN-γ), interleukin (IL)-1β, IL-2, IL-5, IL-6, IL-7, IL-8, IL-8 human antibody (HA), IL-10, IL-12/IL-23p40, IL-15, IL-16, IL-17A, C-X-C motif chemokine ligand 10 [CXCL10 (interferon gamma-induced protein or IP10)], monocyte chemoattractant protein (MCP)-1, MCP-4, macrophage-derived chemokine (MDC), macrophage inflammatory protein (MIP)-1α, MIP-1β, the thymus- and activation-regulated chemokine [CCL17 (thymus- and activation-regulated chemokine or TARC)], tumor necrosis factor (TNF)-β, and vascular endothelial growth factor A (VEGF-A). Assays were performed according to the manufacturer's protocol (Meso Scale Discovery), using a serial dilution of purified analyte (Cytokine 24-Plex Kit) as a standard curve. The electrochemiluminescent signals were detected using a Meso QuickPlex SQ 120 instrument and associated analysis software [Meso Scale Discovery Workbench software (version 4.0)]. Samples were assayed in duplicate and average levels were used for analysis. Individual Baseline levels prior to exposure were averaged across the two Baseline samples. Any sample with an intensity that was not within the linear portion of the standard curve was imputed with the half of the lowest fitted value detected on the Meso Scale Discovery Workbench software.

MR Image Acquisition

To measure region-specific differences in brain volume and connectivity, 12 animals representing 6 control animals and 6 DA-exposed animals showing evidence of tremoring (0.075-mg/kg BW per day group, $n=2$; 0.15-mg/kg BW per day group, $n=4$) were selected for imaging in the Postpartum period (Table S1). Animals were sedated with ketamine [5–10 mg/kg BW intramuscular (IM)] and atropine (0.04 mg/kg IM), then intubated and maintained on inhaled sevoflurane (0.8%–2.5%) and 100% oxygen throughout the acquisition period (~ 1 h). Vitals (heart rate and saturated oxygen) were closely monitored for the duration. MR scans were acquired during a single scan using a 3T Scanner (version 5.17; Philips) with a custom-made 8-channel radiofrequency head coil that was developed and optimized for the nonhuman primate head by C. Hayes at the University of Washington Department of Radiology.[55]

High-resolution, three-dimensional, T1-weighted magnetization-prepared 180 degrees radio-frequency pulses and rapid gradient-echo (MPRAGE) images were acquired using a multi-shot turbo field echo (TFE) pulse sequence and an inversion prepulse (1,151 ms delay); repetition time (TR)/echo time (TE) = 14 ms/7.1 ms; 130 axial slices; acquisition matrix $208\times141\times130$; acquisition voxel size $0.48\times0.53\times1.0$ mm; reconstructed voxel size $0.39\times0.39\times0.5$ mm; slice over sample factor = 2; sense factor = 2 in the foot–head direction; turbo factor = 139; number of signaling averages = 1; TFE shots = 65, and acquisition time = 3 min 14 s. Diffusion-weighted images were acquired with the following parameters: spin-echo echo-planar pulse sequence with diffusion gradients, repetition time = 5,500 ms, echo time = 77.98 ms, reconstructed matrix 128×128, number of slices 44, resolution/voxel size $0.78\times0.78\times1.5$ mm, 64 different diffusion-weighted directions and one nondiffusion volume at Blip right, b value of 1,500, 5 different diffusion-weighted directions and one nondiffusion volume at Blip left, which were compatible with *FSL*'s (FMRIB Software Library; version 6.0) *topup* and *eddy* software.[56]

T1 Image Processing

In *FSL*, FMBIR's Linear Image Registration Tool (*FLIRT*; https://fsl.fmrib.ox.ac.uk/fsl/fslwiki/FLIRT)[57–59] was used to coregister all T1 images from the animals to a single target brain randomly selected from the group of images. The *buildtemplate* and *WarpImageMultiTransform* command from *ANTs* (Advanced Normalization Tools; version 2.3.2), were used to coregister all T1 images in common space,[60] along with a labeled *Macaca mulatta* T1 atlas.[61] Labeled atlases were then inverse transformed into the original space of the 12 individual animals, using nearest-neighbor options. In individual space, *FSLmaths* was used to extract each region of interest (ROI) from the individual atlases. ROI volumes from the left and right hippocampus and thalamus were extracted using *FSLstats*.

Diffusion Tensor Image Processing

Diffusion tensor images (DTIs) were processed using *FSL*'s *topup* software and *FSL*'s *eddy* software to minimize distortion from eddy currents and head motion.[56,62] The *FSL* program, *dtifit* (https://fsl.fmrib.ox.ac.uk/fsl/fslwiki/FDT), was used to reconstruct the diffusion tensor for each voxel, and the matrix was diagonalized to obtain tensor eigenvalues, L1, L2, L3. *ANTs's*

buildtemplate[60] was used to coregister individual FA maps to a target brain. Seed points were hand drawn in the hippocampus and thalamus in the viewing system, *FSLeyes* (version 0.30.0), and masks of the common space seed points were inverse transformed into original space. Using these seed points, *probtrackx* in *FSL* was used to generate probabilistic diffusion tractography to assess connectivity between the hippocampus and thalamus.[63] This measure takes into account intra-voxel crossing fibers and allows for an estimate of the myelin pathways that originate at any specific voxel and pass through any specific other voxel.[63]

MR Imaging Analysis

Volumes from each brain ROI were exported to R (version 4.0; R Development Core Team). Comparisons of volume were conducted on control vs. DA-exposed animals, using a two-tailed Student's *t*-test, to maximize statistical power. A Bonferroni correction was applied to the *p*-values to account for the multiple comparisons made for the number of brain regions assessed. Significance was set at a corrected $p < 0.05$. Connectivity between the hippocampus and thalamus was compared using *FSL* software *randomise*, a method that uses 500 random permutations and threshold-free cluster enhancement (TFCE) to correct for multiple voxel comparisons.[64,65] Permutations were used to compare connectivity between groups. Any significant alterations in region-specific connectivity, as identified with a $p < 0.05$, were visually identified in the brain as a cluster in *FSLeyes*.

Tissue Collection

Animals were fasted for 12 h prior to sedation under ketamine (20 mg/kg IM), before transportation to the necropsy room at the University of Washington National Primate Research Center (WaNRPC). Sedated animals were euthanized with an overdose of sodium pentobarbital (390 mg IV), as per the American Veterinary Medical Association Panel on Euthanasia recommendations.[66] Euthanasia was confirmed by veterinary staff. The brain was quickly excised from the skull and bisected along the midsagittal plane. Distinct brain regions containing the fimbria, internal capsule, hippocampus, fornix, and thalamus were identified by a certified veterinary pathologist for collection. Sections from the right hemisphere were immersion fixed in 10% formalin. From the left hemisphere, dissected tissue was sliced into small, ~3-cm sections (representing 1–3 sections/region), placed in a 5-mL tube, immediately frozen in liquid nitrogen, and stored at −80°C.

Histology and Immunohistochemistry

To maintain tissue handling consistency, formalin-fixed sections containing the fimbria, internal capsule, hippocampus, fornix, and thalamus from 28 animals (control group, $n = 8$; 0.075-mg/kg BW per day group, $n = 11$; 0.15-mg/kg BW per day group, $n = 9$; see Table S1 for details), were processed through a graded series of ethanol and embedded in paraffin. To standardize timing and processing across animals, the order of sectioning, clearing, and staining followed a counterbalanced paradigm for exposure to ensure uniform handling of sections representing any one region. Paraffin-embedded sections were serial sectioned at 10 μm. Sections were deparaffinized in xylene, rehydrated in distilled water, and stained for general cellularity with hematoxylin and eosin (H&E). Cytoplasmic staining of Nissl substance in neuronal cytoplasm was conducted with cresyl violet (CV; Poly Scientific). Myelin was stained with Luxol fast blue (LFB; Rowley Biochemical Inc.), a copper phthalocyanine dye attracted to bases found in the lipoproteins of the myelin sheath.[67] Myelin fibers appear blue and the stain is commonly used to detect demyelination or hypomyelination in the central nervous system (CNS) based on staining intensity.[68] Sections were incubated overnight at 57°C with 0.1% LFB solution followed by a 95% alcohol rinse and a distilled water rinse, then differentiated with 0.05% lithium carbonate (Poly Scientific) and 70% alcohol, and counterstained with CV. Sections were dehydrated through graded ethanol, cleared in xylene, and coverslipped.

For immunohistochemistry, endogenous peroxidase was blocked using 3% hydrogen peroxide followed by heat-induced epitope retrieval using a 10 mM citrate buffer solution, pH 6.0, in a Decloaker pressure chamber (Biocare Medical) for 15 min at 110°C. Nonspecific staining was blocked using 10% normal goat serum (Jackson Immunoresearch) for 20 min at ~23°C [room temperature (RT)] and an avidin/biotin blocking kit (Vector Laboratories). To identify microglia, sections were incubated with rabbit monoclonal anti-ionized calcium binding adaptor molecule 1 (Iba-1) (1:2,000; Cat# 019-19,741, Lot# CAL0291, Wako Chemicals USA) for 60 min at RT followed by incubation with biotinylated goat anti-rabbit IgG antibody (1:300; Vector Laboratories) 30 min at RT. To identify astrocytes, sections were incubated with an antibody to the structural protein, glial fibrillary acidic protein (GFAP), rabbit anti-GFAP (1:7,000, Cat# X0936, Lot# 200256262, Dakocytomation Corp.), for 30 min at RT then incubated with biotinylated goat anti-rabbit IgG (Vector Laboratories) at a 1:500 dilution. Antigen–antibody complexes were visualized with a Vectastain Elite ABC R.T.U. label (Vector Laboratories,) and 3,3′-diaminobenzidine (Dakocytomation Corp.). Iba-1$^-$ controls were stained with normal rabbit IgG (1:400; Calbiochem/EMD Millipore) and GFAP$^-$ controls were stained with rabbit immunoglobulin fraction (solid phase adsorbed) control (Dakocytomation Corp.). Sections were counterstained with hematoxylin and coverslipped.

Sections for each animal and region were scanned under 40× magnification using an Aperio ScanScope AT2 DX System (Leica Biosystems Imaging Inc.) and viewed using Aperio ImageScope (version 6.25.0.1117). The hippocampus (CA1, CA3–4, and dentate gyrus), thalamus, fornix, fimbria, and internal capsule were identified using the *Macaca mulatta* BrainMaps labeled atlas.[69] These regions were selected to include specific target regions known to be vulnerable to DA neurotoxicity and white matter tracts previously shown by MR imaging of these animals to have lower structural integrity.[43] Hippocampal coordinates were identified on coronal sections as A0.4–A15.0, at 27.5–36.5 mm deep, and 8.5–21.5 mm from the midsagittal plane. The fornix coordinates were P1.7–A16.1, at 16–30 mm deep and 0–16.5 mm from the midsagittal plane. The internal capsule coordinates were A1.3–A20.6, at 15–26.5 mm deep and 3.5–20 mm from the midsagittal plane. Atlas coordinates for fornix connections to the hippocampus were A0.4–A0.6, and for fimbria connections, A0.9–A12.0. The fornix and fimbria were visually differentiated by the corresponding shape of the dentate gyrus and surrounding CA1–4 regions. Images were evaluated across 4× – 40× magnifications to capture overall regional staining.

Immunoreactivity Assessment

Following visual examination of immunostaining for Iba-1 and GFAP in the fimbria, internal capsule, hippocampus, fornix, and thalamus, sections from three controls and four DA-exposed animals were selected and confirmed for match to orientation of cut by distinct anatomical features.[69] A defined ROI (800 μm^2) was identified, and, within each ROI, 20 microglia were randomly selected, representing cells displaying the cell soma and processes. Cell soma area was determined using the Aperio software program for quantification (Leica Biosystems). The morphological phenotype of these 20 microglia was ranked using a rating scale reflective of surveillant to ameboid reactive phenotypes (Figure 2). To address issues of possible selection bias of the

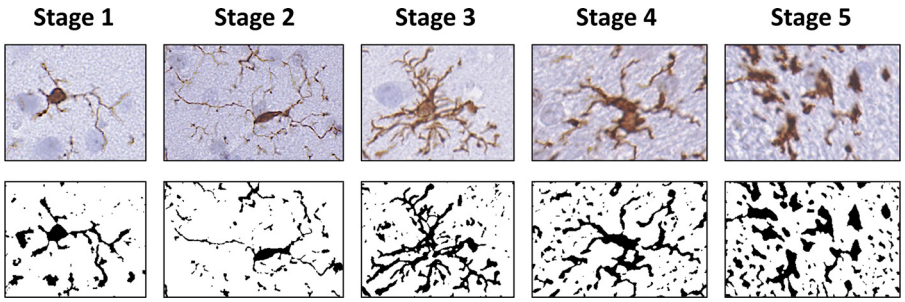

Figure 2. Representative rating scale (1–5) for Iba$^+$microglia morphology, as collected across the experimental brain regions examined. Images represent skeletonized Iba-1$^+$microglia and their assigned rating score as it related to the progressive change in morphology. Briefly, stage 1 represents cells that had light cytoplasmic staining and limited branched processes; stage 2 represents cells that showed longer process and more branching; stage 3 represents cells that showed denser staining morphology but maintained long processes; stage 4 represents cells that showed thicker and shortened processes; stage 5 represents ameboid microglia that were almost globose and bore limited short processes. Note: Iba-1, ionized calcium binding adaptor molecule 1.

matched sections of the thalamus, sections from additional animals containing the thalamus in a different plane of cut were randomly examined and comparable cell soma size was confirmed.

GFAP$^+$astrocytes were evaluated for cell soma staining using a morphological ranking pattern outlined in human aging studies.[70] Assessment of astrocytes within an ROI (500 μm^2) was limited to morphological ranking only.[70] Cells were classified as type 1 for cells with light cytoplasmic staining and slender processes, type 2 for cells with visually higher levels of GFAP immunoreactivity, larger soma, and slightly thick processes, or type 3 for cells showing hypertrophy and with larger soma and prominent GFAP immunoreactivity. In the hippocampus, subregional representation of the dentate gyrus was available across all sections.

RNAseq

Total RNA was isolated from the hippocampus of the left hemisphere from six control animals and five DA-exposed animals (0.075-mg/kg BW per day group, $n = 2$; 0.15-mg/kg BW per day group, $n = 3$; see Table S1 for details), using a Qiagen miRNeasy Kit (Qiagen) according to manufacturer's protocol. RNA purity was assessed using a NanoDrop ND-1000 Spectrophotometer (Thermo Fisher Scientific) and RNA integrity was determined using the Agilent RNA 6000 Nano Kit with an Agilent 2100 Bioanalyzer. RNA samples with RNA integrity number (RIN) > 7 were used for RNA-Seq analysis.

Complementary DNA cDNA libraries were prepared from 1 µg of polyA RNA using the TruSeq Stranded mRNA kit (Illumina) and the Sciclone NGSx Workstation (Perkin Elmer). Prior to cDNA library construction, ribosomal RNA was removed by means of poly A enrichment. Each library was uniquely barcoded and subsequently amplified over a total of 13 cycles of polymerase chain reaction (98°C for 10 s, 60°C for 30 s, 72°C for 30 s; following the final cycle, samples were kept at 72°C for 5 min and then held at 10°C). Library concentrations were quantified using Qubit fluorometric quantitation (Life Technologies). Average fragment size and overall quality were evaluated with the DNA1000 assay on an Agilent 2100 Bioanalyzer. Each library was sequenced with paired-end 100-bp reads to a minimum depth of 30 million reads on an Illumina NovaSeq 64000 sequencer. Sequences were aligned with the National Center for Biotechnology Information (NCBI) *M. fascicularis* genome (Macaca_fascicularis_5.0) by the salmon aligner (version 1.2.1) with the following parameters: –validateMappings –incompatPrior 1 –p 30 –useVBOpt –gcBias –posBias –biasSpeedSamp 10. Transcript counts were read into R using the Bioconductor *tximport* package, summarizing transcript (NCBI RefSeq transcript) counts at the gene (NCBI Gene identifier) level using length-scaled transcript per million (TPM) abundances.

The differences in gene expression between exposed and control conditions were assessed using limma-voom pipeline from the Bioconductor *limma* package[71] in R (version 4.0; R Development Core Team). Counts were scaled by effective library size and then $\log_2$ transformed (log counts per million), after which a mean-dependent variance estimate was computed for each observation, the inverse of which was used as an observation-level weight to control for the mean–variance dependence structure. There were incomplete replicate measures for each animal, so data were analyzed using a weighted linear mixed model to account for intra-animal correlations.[72] Comparisons between groups (limited to exposed or control groups, owing to the low sample size available) were made using empirical Bayes adjusted contrasts, and the resulting p-values were adjusted using the Benjamini and Hochberg method to control the false discovery rate (FDR).[73] Genes with $\log_2$ fold change (FC) > 1.5 and $p < 0.05$ were considered as significantly differentially expressed genes (DEGs), and the most significant genes were identified with the additional consideration of an FDR q-value of 0.05. The sequencing data were deposited to Gene Expression Omnibus with the accession number GSE163026.

To compare results across other published data, two comparisons were made: one for DEGs related to DA exposure, and one for DEGs known to be associated with neuronal and glial cells. A literature search was conducted to identify any genome-wide studies reporting DEGs in the CNS. Three studies that met these criteria were identified: one with acute DA exposure in mice[74] and two others with acute[75] or chronic[76] exposure in zebrafish. Genes linked to neural cells (including neurons and astrocytes) were taken from the transcriptome database outlined by Cahoy et al.[77] Coefficients from other studies' DEGs were extracted and directionally compared with matching orthologs in the present study.

Functional Enrichment Analysis for RNAseq

Gene Set Enrichment Analysis (GSEA; version 4.1) was performed to assess functional enrichment in significant genes.[78,79] Targeted gene sets were developed (Table S2). Genes involved in neuronal health, inflammation, or white matter and myelin as generated from a published transcriptional database on these cell types,[77] and excitoxicity genes were based on results from Pappas et al.[80] RNAseq data and from literature searches were assembled and input into GSEA. Using all ranked transcripts, 1,000 permutations were applied to assess the significance of gene sets. As recommended by the GSEA User Guide (https://www.gsea-msigdb.org/gsea/doc/GSEAUserGuideFrame.html), gene sets with FDR $q < 0.25$ were considered as significantly enriched.

Table 1. Median complete blood count measures (range).

	Baseline			Initial exposure		
	Controls ($n=8$)	0.075 mg/kg per day ($n=10$)	0.15 mg/kg per day ($n=10$)	Controls ($n=8$)	0.075 mg/kg per day ($n=10$)	0.15 mg/kg per day ($n=10$)
WBC (thousand/μL)	11.1 (7.1–12.3)	9.3 (6.6–12.5)	9.5 (5.7–13.2)	9.5 (5.7–13.2)	9.0 (6.3–15.7)	9.0 (4.5–13.2)
RBC (million/μL)	5.3 (5.2–5.7)	5.2 (4.8–5.7)	5.0 (4.2–5.5)	5.3 (4.6–6.0)	5.4 (4.5–5.9)	4.8 (4.6–5.7)
HGB (g/dL)	12.5 (11.2–14.0)	11.9 (10.2–13.5)	12.1 (10.7–13.4)	12.2 (10.6–15.0)	11.9 (10.6–13.6)	12.0 (9.3–14.4)
HCT (%)	42.0 (37.0–45.0)	40.0 (33.0–44.0)	39.0 (34.0–45.0)	41.0 (35.0–47.0)	39.0 (35.0–43.0)	40.0 (32.0–46.0)
MCV (fL)	78.0 (72.0–80.0)	75.0 (66.0–79.0)	81.0 (74.0–83.0)	78.0 (73.0–80.0)	74.5 (66.0–77.0)	79.0 (70.0–83.0)
MCH (pg)	23.8 (21.6–24.6)	23.4 (20.2–24.7)	24.5 (22.1–31.9)	23.5 (21.5–24.9)	22.8 (20.2–24.2)	23.8 (20.1–25.6)
PLT (thousand/μL)	389.0 (256.0–540.0)	503.5 (270.0–569.0)	393.0 (338.0–526.0)	385.0 (290.0–529.0)	461.0 (263.0–601.0)	432.0 (304.0–506.0)
Neut (thousand/μL)	5.0 (2.7–8.0)	4.4 (2.2–6.5)	3.7 (2.2–7.9)	5.2 (1.6–8.6)	3.4 (2.1–9.1)	2.8 (1.5–5.3)
Lymph (thousand/μL)	4.5 (2.7–8.0)	3.8 (2.8–6.5)	3.9 (1.4–6.7)	3.8 (2.0–7.5)	3.9 (3.0–6.2)	5.5 (2.0–8.1)
Mono (thousand/μL)	0.3 (0.3–0.6)	0.5 (0.3–0.9)	0.5 (0.2–1.1)	0.5 (0.3–1.6)	0.5 (0.2–0.8)	0.4 (0.2–0.9)
Eos (thousand/μL)	0.1 (0.0–0.4)	0.1 (0.0–0.5)	0.1 (0.0–0.4)	0.1 (0.0–0.5)	0.2 (0.0–1.1)	0.1 (0.1–0.4)

Note: Median complete blood count measures plus range in parentheses. Initial exposure time point was at day 73 of exposure. Basophils were counted for all animals and recorded at 0 thousand/μL. No significant changes were observed across dose groups when comparing individual differences in measures using a one-way ANOVA. ANOVA, analysis of variance; Eos, eosinophil, HCT, hematocrit; HGB, hemoglobin; Lymph, lymphocytes; MCH, mean corpuscular hemoglobin; MCV, mean corpuscular volume; Mono, monocytes; Neut, neutrophils; PLT, platelet blood count; RBC, red blood cells; WBC, white blood cells.

Statistical Analyses

Quantified CBC measures and chemistry analytes were imported into R (version 4.0; R Development Core Team). Individual animal relative changes of initial exposure and baseline were calculated for each analyte to account for individual animal variances. Bartlett's test was used to determine homogeneity of variance. Dose effects of relative changes from baseline for CBCs and clinical chemistry analytes, and microglia soma size, were analyzed using a one-way analysis of variance (ANOVA). Dose effects and the interaction effects of dose over time of relative changes from Baseline for the cytokine and chemokines were analyzed using a one-way, repeated-measures ANOVA. The categorical rating scale data were analyzed by a chi-square test. Significance was set at a Bonferroni-corrected $p < 0.05$ using two-tailed tests. Group n sizes are provided in figure legends or tables.

Results

Previously Reported General Health Assessments

As previously reported,[39] the DA exposure schedule and dose did not result in differences in BWs or general observational clinical health assessments. There was no effect on conception or successful pregnancy. No differences were observed in reactivity, visual orientation, visual tracking, and reaching. Tremors with reaching were associated with DA exposure.

CBC and Clinical Chemistry

CBC and serum chemistry values were examined by WaNRPC veterinarians and determined to be within normal, healthy ranges. Detection of nucleated RBCs was limited, and this measure was excluded from the analysis. Levels of detection for all other CBC and serum chemistry measures were acceptable in all samples. No differences in changes of CBC (Table 1) and clinical chemistry measures (Table 2) were observed between DA-exposed groups and controls.

Cytokine and Chemokine Blood Levels

Thirteen analytes [Eotaxin-3, GM-CSF, IFN-γ, IL-1β, IL-2, IL-5, IL-6, IL-8, IL-8 (HA), IL-10, IL-17A, TARC, and TNF-β] had >80% of samples below the LOD and were not statistically analyzed. Levels of IL-7, IL-12/IL-23p40, IL-15, IL-16, CXCL10

Table 2. Median serum chemistry measures (range).

	Baseline			Initial exposure		
	Controls ($n=7$)	0.075 mg/kg per day ($n=10$)	0.15 mg/kg per day ($n=9$)	Controls ($n=7$)	0.075 mg/kg per day ($n=10$)	0.15 mg/kg per day ($n=9$)
Sodium (mEq/L)	143.0 (141.0–146.0)	143.0 (141.0–148.0)	144.0 (141.0–147.0)	144.5 (141.0–148.0)	144.0 (143.0–148.)	145.0 (144.0–146.0)
Potassium (mEq/L)	3.6 (3.3–4.0)	3.7 (3.2–4.7)	3.6 (3.3–4.1)	3.8 (3.0–5.2)	3.6 (3.0–4.2)	3.8 (3.1–4.6)
Chloride (mEq/L)	105.0 (103.0–107.0)	105.5 (102.0–109.0)	107.0 (104.0–109.0)	107.5 (106.0–113.0)	109.0 (105.0–112.0)	109.0 (107.0–113.0)
Calcium (mg/dL)	9.8 (9.6–10.0)	10.0 (9.5–10.3)	9.3 (8.8–10.4)	9.6 (9.2–10.6)	9.6 (8.9–10.6)	9.3 (8.1–10.1)
Phosphate (mg/dL)	4.7 (2.9–5.8)	4.9 (2.9–6.2)	4.2 (2.0–5.1)	3.6 (2.4–5.3)	3.8 (1.8–5.3)	3.2 (2.1–4.4)
Cholesterol (mg/dL)	119.5 (96.0–167.0)	129.5 (81.0–167.0)	124.5 (76.0–154.0)	125.0 (116–223.0)	148.5 (105.0–201.0)	132.5 (112.0–181.0)
ALT (U/L)	31.5 (20.0–46.8)	32.0 (20.0–51.0)	33.5 (10.0–51.0)	36.0 (25.0–126.0)	28.5 (20.0–69.0)	34.5 (16.0–44.0)
AST (U/L)	36.0 (29.0–48.0)	38.5 (28.0–57.0)	39.5 (26.0–61.0)	37.0 (26.0–74.0)	30.0 (16.0–67.0)	38.5 (26.0–81.0)
GGT (U/L)	52.5 (39.0–71.0)	46.0 (36.0–61.0)	51.5 (24.0–73.0)	50.0 (37.0–62.0)	41.5 (33.0–58.0)	45.0 (22.0–69.0)
Glucose (mg/dL)	61.0 (49.0–77.0)	65.5 (51.0–73.0)	61.0 (41.0–81.0)	47.0 (13.0–75.0)	55.5 (24.0–91.0)	55.0 (15.0–76.0)
Blood urea nitrogen (mg/dL)	22.0 (17.0–28.0)	20.5 (19.0–26.0)	21.0 (14.0–27.0)	20.5 (15.0–24.0)	21.0 (13.0–25.0)	20.5 (17.0–30.0)
Creatinine (mg/dL)	0.7 (0.6–1.0)	0.7 (0.6–0.8)	0.7 (0.6–0.9)	0.7 (0.6–0.8)	0.8 (0.6–0.9)	0.6 (0.6–0.8)
Total protein (g/dL)	7.0 (6.3–7.6)	7.2 (6.6–7.5)	7.1 (6.0–7.8)	6.7 (6.1–7.8)	7.0 (6.2–8.0)	6.8 (5.3–7.5)
Albumin (g/dL)	4.0 (3.5–4.3)	4.0 (3.8–4.1)	3.8 (2.9–4.7)	3.8 (3.4–4.0)	3.9 (3.6–4.2)	3.7 (2.2–3.9)
Globulin (g/dL)	3.0 (2.7–3.3)	3.3 (2.5–3.5)	3.2 (2.5–4.3)	3.0 (2.4–3.9)	3.1 (2.6–4.1)	3.2 (2.4–3.8)
Total bilirubin (mg/dL)	0.2 (0.1–0.3)	0.2 (0.1–0.2)	0.2 (0.1–0.3)	0.2 (0.1–0.2)	0.2 (0.1–0.2)	0.2 (0.1–0.3)
Alkaline phosphatase (U/L)	122.5 (107.0–354.0)	174.5 (87.0–328.0)	119.0 (67.0–204.0)	116.5 (73.0–213.0)	147.0 (96.0–199.0)	108.5 (68.0–134.0)

Note: Median serum chemistry measures plus range in parentheses. Initial exposure time point at day 73 of exposure. No significant changes were observed across dose groups when comparing individual differences in measures using a one-way ANOVA. ALT, alanine transaminase; ANOVA, analysis of variance; AST, aspartate aminotransferase; GGT, gamma-glutamyl transferase.

Table 3. Median cytokine and chemokine measures (range).

	Dose group[a]	Baseline	Initial exposure 1	Initial exposure 2	Necropsy
IL-7	Controls ($n=7$)	0.74 (0.35–1.86)	0.90 (0.27–2.31)	0.38 (0.19–1.15)	0.37 (0.20–13.29)
	0.075 ($n=3$)	0.75 (0.61–1.68)	1.08 (0.61–1.38)	0.98 (0.91–3.68)	1.22 (0.63–1.49)
	0.15 ($n=6$)	0.92(0.27–6.95)	1.67 (0.38–9.93)	1.13 (0.57–2.32)	0.80 (0.21–2.27)
IL-12p40	Controls ($n=7$)	96.40 (52.79–182.60)	126.78 (48.60–179.33)	121.26 (50.47–227.91)	66.87 (32.20–125.55)
	0.075 ($n=3$)	49.31 (36.24–80.50)	39.28 (38.38–92.43)	60.61 (42.62–70.51)	48.04 (27.45–64.73)
	0.15 ($n=6$)	89.53 (37.85,159.21)	107.10 (44.16–140.18)	85.09 (31.77–204.71)	97.66 (51.94–158.40)
IL-15	Controls ($n=7$)	5.31 (4.86–7.12)	5.73 (5.31–7.29)	5.75 (4.65–8.47)	5.84 (4.50–6.71)
	0.075 ($n=3$)	5.30 (4.90–6.20)	4.31 (4.06–5.15)	5.15 (3.98–5.17)	5.34 (4.18–6.85)
	0.15 ($n=6$)	4.74 (3.95–8.31)	4.97 (3.59–7.04)	4.44 (3.81–9.13)	4.65 (4.08–5.07)
IL-16	Controls ($n=7$)	13.68 (8.50–28.33)	15.37 (14.13–24.24)	19.53 (7.81–24.39)	17.93 (8.02–83.41)
	0.075 ($n=3$)	13.67 (8.21–39.48)	16.32 (6.36–46.63)	7.33 (5.91–15.70)	38.70 (23.54–54.61)
	0.15 ($n=6$)	6.60 (2.99–22.72)	9.66 (7.78–852.96)	5.31 (3.64–18.65)	7.18 (2.10–13.11)
IP-10	Controls ($n=7$)	154.19 (110.02–261.05)	165.03 (106.36–188.35)	151.78 (120.88–253.95)	190.08 (120.63–384.88)
	0.075 ($n=3$)	226.48 (182.16–279.34)	154.23 (132.17–192.74)	247.80 (168.34–558.66)	166.03 (121.70–497.51)
	0.15 ($n=6$)	215.82 (113.25–1542.30)	169.61 (112.39–2870.78)	227.48 (96.50–285.18)	187.04 (150.55–847.08)
MCP-1	Controls ($n=7$)	35.88 (24.06–55.10)	38.12 (24.96–51.04)	36.21 (24.07–44.63)	27.61 (14.52–42.46)
	0.075 ($n=3$)	40.48 (33.29–56.33)	31.80 (26.31–40.68)	32.57 (31.63–49.92)	31.50 (26.97–45.60)
	0.15 ($n=6$)	33.41 (21.12–43.88)	33.10 (26.61–37.81)	38.32 (19.71–46.20)	29.01 (21.17–51.44)
MCP-4	Controls ($n=7$)	74.50 (11.73–152.45)	58.32 (8.82–105.24)	57.23 (5.07–91.75)	69.65 (9.69–92.85)
	0.075 ($n=3$)	76.00 (61.01–94.94)	74.79 (52.28–87.74)	106.27 (58.30–112.84)	50.90 (41.03–56.22)
	0.15 ($n=6$)	57.09 (19.57–71.52)	40.85 (24.89–70.42)	37.69 (24.89–110.81)	36.06 (14.90–67.41)
MDC	Controls ($n=7$)	252.33 (189.63–699.38)	220.24 (197.12–652.52)	279.85 (178.23–546.13)	301.72 (216.92–466.46)
	0.075 ($n=3$)	287.99 (261.95–298.91)	281.24 (243.00–294.76)	292.54 (277.88–357.63)	399.55 (300.25–554.81)
	0.15 ($n=6$)	292.98 (103.34–364.60)	271.85 (136.10–373.51)	230.18 (107.71,351.27)	258.49 (162.63–283.38)
MIP-1α	Controls ($n=7$)	8.85 (5.73–21.81)	10.84 (0.83–21.15)	8.11 (0.83–25.11)	9.04 (0.83–38.70)
	0.075 ($n=3$)	13.50 (7.05–22.42)	19.69 (17.95–34.28)	16.67 (6.61–27.89)	14.10 (9.65–23.91)
	0.15 ($n=6$)	7.32 (1.54–25.97)	8.77 (0.83–25.40)	5.16 (0.83–22.71)	10.66 (0.83–20.81)
MIP-1β	Controls ($n=7$)	49.59 (34.70–70.27)	43.58 (34.99. 66.16)	34.08 (30.65–60.87)	52.32 (27.03–62.75)
	0.075 ($n=3$)	45.24 (41.79–83.86)	61.88 (37.57–64.54)	45.81 (42.02–70.68)	48.61 (37.48–49.80)
	0.15 ($n=6$)	32.33 (30.00–78.56)	34.81 (29.69–77.07)	33.04 (28.78–63.91)	35.04 (28.38–47.14)
VEGF-A	Controls ($n=7$)	3.89 (2.70–4.52)	3.41 (2.40–4.90)	3.16 (1.62–4.34)	5.47 (4.17–7.27)
	0.075 ($n=3$)	5.81 (3.62–6.45)	6.65 (3.16–7.88)	6.17 (3.45–8.81)	11.94 (5.15–13.58)
	0.15 ($n=6$)	4.48 (1.45–139.73)	5.46 (2.35–109.55)	5.71 (2.53–150.65)	8.28 (4.62–97.73)

Note: Units for all analyte data are in picograms per milliliter (pg/mL). Median cytokine and chemokine measures plus range in parentheses. Initial exposure 1 was at day 15 of exposure; Initial exposure 2 was at day 43 of exposure; necropsy was at an average of 425 d of exposure. Analytes with <20% of samples below the limit of detection are not included [eotaxin-3, granulocyte-macrophage colony-stimulating factor (GM-CSF), interferon gamma (IFN-γ), interleukin (IL)-1β, IL-2, IL-5, IL-6, IL-8, IL-8 (HA), IL-10 IL-17A, CCL17 (TARC), tumor necrosis factor (TNF)-β]. No significant changes were observed across dose groups when comparing individual differences in measures using a repeated-measures one-way ANOVA. ANOVA, analysis of variance; IP, interferon gamma-induced protein; MCP, monocyte chemoattractant protein; MDC, macrophage-derived chemokine; MIP, macrophage inflammatory protein; TARC, thymus- and activation-regulated chemokine; VEGF-A, vascular endothelial growth factor A.
[a]Domoic acid exposure in milligrams per kilograms body weight per day (mg/kg BW per day).

(IP10), MCP-1, MCP-4, MDC, MIP-1α, MIP-1β, and VEGF-A were similar across groups prior to the start of exposure. There were no effects of changes in levels that were associated with dose or with dose over time, relative to Baseline at 2 wk, 6 wk, or necropsy (Table 3).

MR Volume and Tractography

MR T1-weighted images were used to calculate the volume of key gray matter structures associated with DA neurotoxicity, including the hippocampus and thalamus. Results from the volumetric analyses did not indicate significant differences in total cellular volume in either the left or right hemisphere of gray matter structures in DA-exposed animals as compared with control animals. Mean hippocampal volume of the right hemisphere was 393.4 ± 14.3 cc for the vehicle controls, 385.8 ± 12.5 cc for DA-exposed animals; left hippocampal volume was 402.6 ± 15.8 cc for controls and 381.0 ± 15.6 cc for DA-exposed animals; right thalamic volume was 496.1 ± 14.8 cc for controls and 513.8 ± 17.9 cc for DA-exposed animals; and left thalamic volume was 501.2 ± 18.3 cc for controls and 515.8 ± 20.2 cc for DA-exposed animals (Figure 3). DTI tractography, a measure of the strength and direction of the white matter fibers, between the hippocampus and thalamus was assessed using a threshold clustering permutation to compare exposure differences. Comparison using 500 permutations and TFCE suggested that the strength and direction of the white matter fiber tracts between these structures were not significantly different across groups (i.e., no clusters were identified at a cutoff of $p = 0.05$).

Histology and Immunohistochemistry

General examination of the brain indicated no overt signs of gross pathology or abnormal color or differences in tissue size. Histological examination of the fimbria, internal capsule, fornix, nucleus accumbens, hippocampus, and thalamus showed a normal pattern of H&E staining with no evidence of eosin$^+$cells that would be indicative of cell death (Figure 4). Additional examination of CV staining showed Nissl granules dispersed throughout the cytoplasm, with no indication of central chromatolysis (Figures 4–7). The overall LFB staining patterns of myelin in the fimbria, fornix, and internal capsule were qualitatively similar across all animals, suggesting no evidence of demyelination (Figure 4).

Iba-1 immunoreactivity in the fimbria and internal capsule suggested a normal pattern of microglia, showing a similar level of complexity ranking at stage 1 across all animals (Figure 4). In the fornix, Iba-1$^+$cell bodies appeared more prominent in the DA-exposed animals than in the controls; however, the cell processes of both groups all had a similar morphological ranking of stage 1. Given the sparse number of cell bodies throughout the fornix, we were unable to confidently quantitate the representative soma size of these cells. In other regions, microglia were quantified in ROIs with ImageScope and rated according to the scale in Figure 2, and group differences were assessed using a

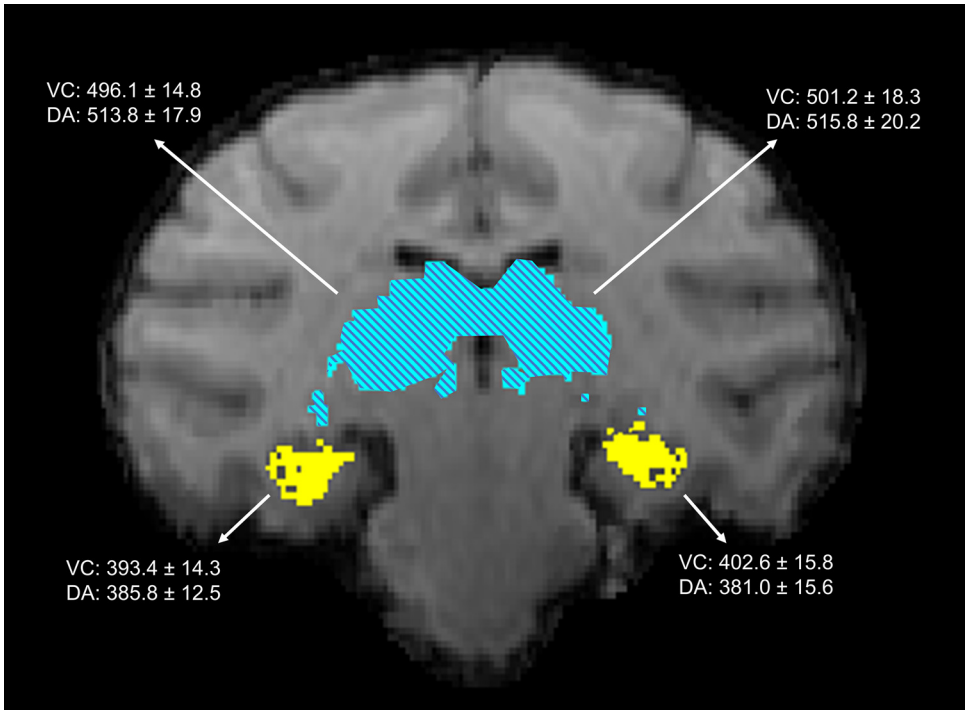

Figure 3. Hippocampus and magnetic resonance (MR) image. A representative coronal slice of an animal with the transformed macaque atlas overlayed in the same space.[69] Highlighted regions show the hippocampus (yellow, solid) in the lower portion of the image and the thalamus (blue, hatched) located within the middle of the image. Inserted data represent the mean volume ± SEM from vehicle control (VC; $n = 6$) and domoic acid-exposed groups (DA; $n = 6$, 2 from the 0.075-mg/kg BW per day group and 4 from the 0.15-mg/kg BW per day group) for each of the sites, as indicated by arrows. No significant differences were observed across the VC and DA groups, using a two-tailed *t*-test. Units are in cc. Note: SEM, standard error of the mean.

chi-square test. In the hippocampus, Iba-1$^+$microglia staining within an 800-μm^2 ROI ranked similarly between controls and DA-exposed animals. Iba-1$^+$microglia displayed a normal pattern of cells with small soma and fine processes across all groups, representative of a stage 1 morphology (Figure 5).

In the thalamus, Iba-1$^+$microglia showed the characteristic morphology of small cell bodies with fine ramified processes in controls. However, in DA-exposed animals, a general morphological phenotype was characterized by larger cell soma and extended primary processes (Figure 6). In the control thalamus ROIs (800 μm^2); the average cell body size was 5.1 μm^2, with a range of 2.6–7.6 μm^2. In DA-exposed animals, an average soma size of 7.2 μm^2, with a range of 4.6–10.2 μm^2, was observed. Of the 20 cells evaluated for soma size in controls, the morphological phenotype followed a pattern of small cell bodies with limited fine processes (100% of cells stage 1). In DA-exposed animals, the cells displayed an extension of processes and ramifications. Most DA-exposed examined cells showed stage 2, representative of the extended processes (80% or 16/20 cells per ROI). The remaining 20% of cells (4/20 cells per ROI) displayed stage 1. There was no evidence of a microglia morphology normally associated with acute neuronal injury.

GFAP$^+$astrocytes showed similar morphology in controls and DA-exposed animals (Figure 4), characterized by small cell soma with thin processes in the fibrous astrocytes of the white matter or by shorter and thicker processes characteristic of protoplasmic astrocytes in the gray matter. In the internal capsule, the staining pattern was similar between control and DA-exposed animals. In the fimbria and fornix, both fibrous and protoplasmic astrocytes were observed. In the thalamus of DA-exposed animals, >50% (range: 10–15 of 20) of the cells examined within the ROI showed denser staining in the cell soma; only in 10% (range: 2–6 of 20) of the cells examined in the controls had similar staining. In the hippocampus, GFAP immunostaining suggested a denser staining pattern in the DA-exposed animals as compared with controls (Figure 7). Assessment of astrocytes within an ROI (500 μm^2) was limited to morphological ranking and compared using a chi-square test. In vehicle controls, GFAP$^+$astrocytes displayed long processes and light staining of the soma (type 1). In the DA-exposed animals, GFAP immunostaining of the cell soma was prominent and representative of type 2. Although the cell body of GFAP$^+$astrocytes in the dentate gyrus of the hippocampus were more prominent with DA exposure, there was no indication of reactive astrocytosis or astrocyte hypertrophy (type 3) (Figure 7).

Sites of Incidental Microglia Reactivity

When reviewing all histology slides, isolated focal events of microglia reactivity/activation were noted in some animals (Figure 8). Identified clusters of Iba-1$^+$microglia showed morphological differences in the fornix, fimbria, thalamus, and nucleus accumbens. Three clusters were in the thalamus of three animals (0.075-mg/kg BW per day group, $n = 1$, 0.15-mg/kg BW per day group, $n = 2$), one of which also showed a cluster in the fornix (0.15-mg/kg BW per day group). Other individual animals each showed one additional cluster in the internal capsule (control), fimbria (0.075-mg/kg BW per day group), and nucleus accumbens (0.075-mg/kg BW per day group). The prominent morphology was consistent with a rating of between stages 3 and 5, as would be expected with a focal response to injury. The associated hematoxylin counterstain showed no indication of ongoing cellular degeneration, and comparable examination in adjacent sections showed no evidence of ongoing localized cell death or astrocyte hypertrophy. H&E staining of these areas in subsequent sections showed no evidence of ongoing congestion or meningeal hemorrhage (Figure S1).

RNA-Seq Transcriptome of the Hippocampus

A global profiling of the 17,734 *Macaca fascicularis* transcripts from the hippocampus of DA-exposed animals (control, $n = 6$;

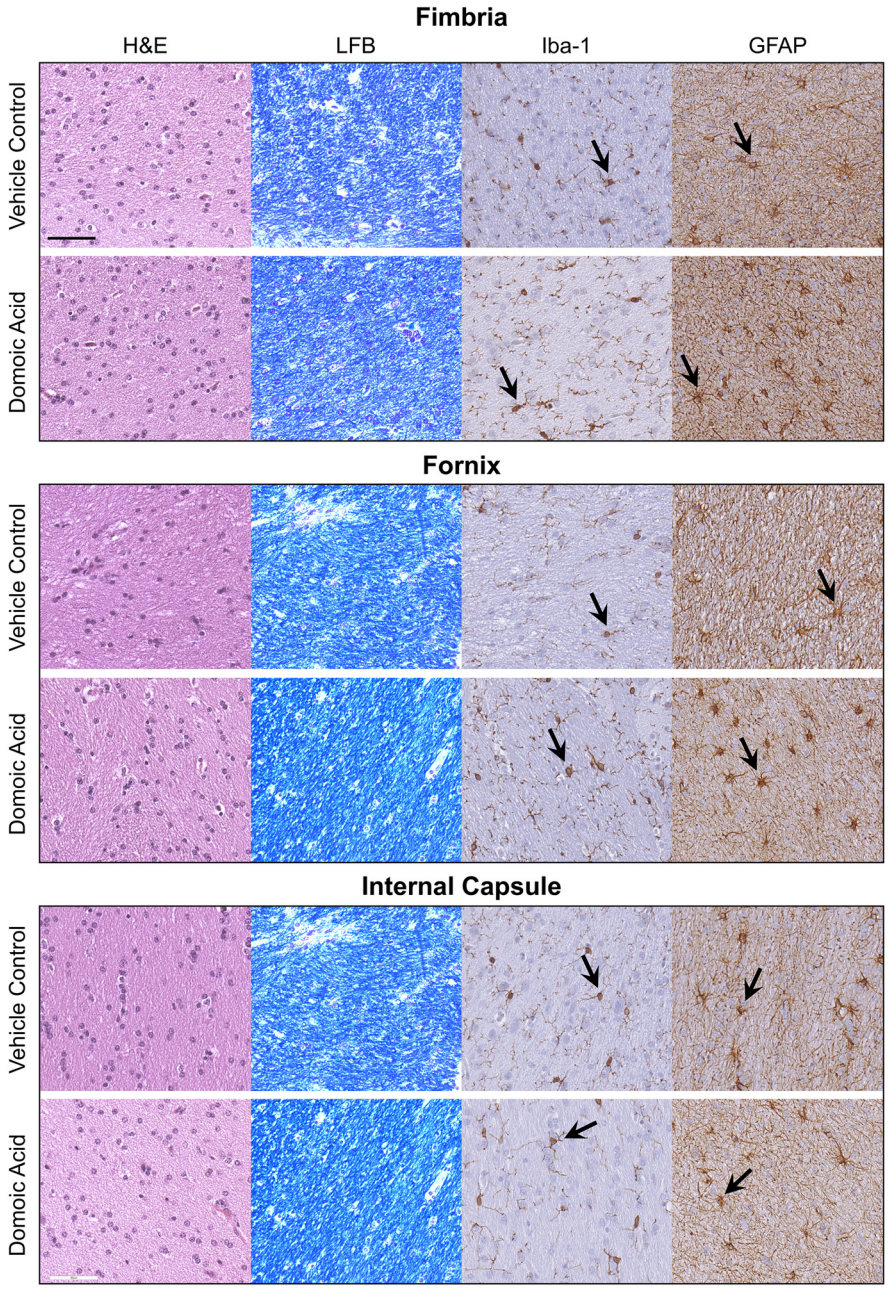

Figure 4. Representative images of staining of 10% formalin-fixed, paraffin-embedded, 10-μm sections of the fimbria, fornix, and internal capsule for general cellularity by hematoxylin and eosin (H&E); myelin by Luxol fast blue (LFB); microglia by ionized calcium binding adaptor molecule 1 (Iba-1; 1:2,000; Wako Chemicals, see arrow); and astrocytes by glial fibrillary acidic protein (GFAP; 1:7,000, Dakocytomation, see arrow) from female *Macaca fascicularis* following prolonged exposed to domoic acid (0.15-mg/kg BW per day) or vehicle (5% sucrose). Scale bar:100 μm.

0.075-mg/kg BW per day group, $n = 2$; 0.15-mg/kg BW per day group, $n = 3$; see Table S1) detected 291 up-regulated and 457 down-regulated transcripts that were suggestive of differential expression (log-FC ≥ 1.5 and $p \leq 0.05$), mapping to 547 unique genes (Figure 9A,B; see Excel Table S1 for unique genes). Of these, 9 DEGs also had an FDR $q < 0.05$ (Figure 9C). Four genes were up-regulated, including chitinase 3 like 1 (*CHI3L1*), early growth response (EGR) 1 (*EGR1*), phospholipid phosphatase 2 (*PLPP2*), and CDC42 effector protein 1 (*CDC42EP1*). Another five genes were down-regulated: phytanoyl-CoA dioxygenase domain containing 1 (*PHYHD1*), integrin subunit beta like 1 (*ITGBL1*), transmembrane protein 100 (*TMEM100*), dopamine receptor D2 (*DRD2*), and vestigial like family member 3 (*VGLL3*).

To compare DEGs (log-FC ≥ 1.5 and $p \leq 0.05$) in the present study to those that have been previously reported, we conducted a literature search for genome-wide studies reporting DEGs in the CNS, ultimately identifying three relevant studies: one with acute DA exposure in mice[74] and two others with acute[75] or chronic[76] exposure in zebrafish. We identified 14 overlapping DEGs between these studies and our data (Figure 9D). Three of these overlapping DEGs were expressed in the same direction as previously reported: fos proto-oncogene (*FOS*) and *EGR4* were up-regulated; regulator of G protein signaling 9 (*RGS9*) was down-regulated. DEGs that have previously been implicated in models of DA toxicity,[74–76] including the early response proto-oncogene, *JUNB,* glutamate receptor genes (of the *GRIA* and *GRIK* families), and genes related to inflammation [genes for

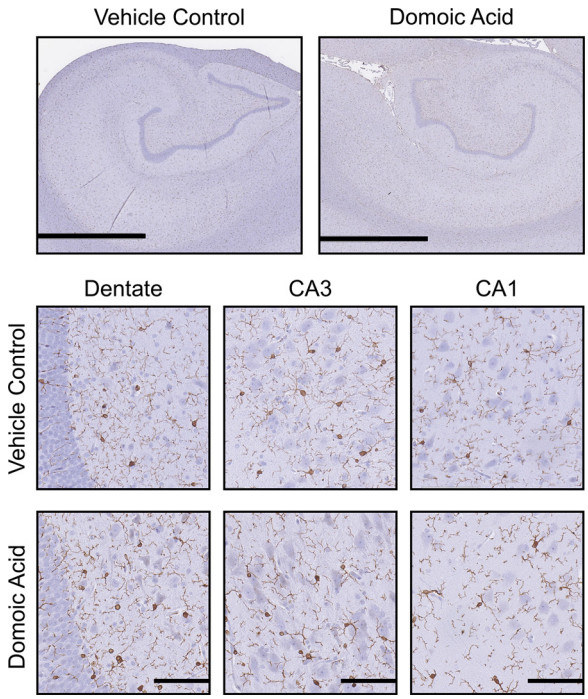

Figure 5. Hippocampal Iba-1 immunoreactivity. Representative images of immunostaining of 10% formalin-fixed, paraffin-embedded, 10-µm sections for Iba-1^{+} (1:2,000; Wako Chemicals) microglia in the hippocampus of female *Macaca fascicularis* following prolonged exposed to domoic acid (0.15-mg/kg BW per day) or vehicle (5% sucrose). Images represent the hippocampus (scale bar: 2,000 µm) and specific hippocampal regions, including the dentate gyrus (scale bars: 200 and 100 µm) and the CA3 and CA1 pyramidal cell layers (scale bar: 100 µm). Immunoreactivity was visualized with Vectastain Elite and shows as darker process-bearing cells within the image. Sections were counterstained with cresyl violet (CV). Note: CA, cornu ammonis area; Iba-1, ionized calcium binding adaptor molecule 1.

cyclooxygenase (COX), S100B, and nuclear factor kappa B (NFκB)], were notably absent from the present study's list of DEGs. There were some suggestions of an up-regulation of genes for the surface receptor expressed by myeloid cells and immune response regulator, *CD300E*, and the glucagon like peptide 2 receptor, *GLP2R*, but these did not meet the FDR q-value cutoff of 0.05. A similar suggestive down-regulation was observed in adenosine receptor gene, *ADORA2A*, insulin-like growth factor 2 (*IGF2*), and IGF binding protein 5 (IGFBP5). One glutamate receptor gene for *N*-methyl-D-aspartate (NMDA)-type receptors (*GRIN2B*) was identified as an up-regulated DEG. No glutamate transporter genes (including *SLC1A1, SLC1A2, SLC1A3, SLC1A6,* and *SLC1A7*) were identified as DEGs.

To gain a better representation of the overall gene profile differences in the hippocampus with DA exposure, GSEA was conducted to identify the pathways represented across the four author-curated lists of genes related to *a*) general neuronal health, *b*) excitotoxicity, *c*) inflammation/glia, and *d*) myelin, axons, and white matter (Table S2). From these curated gene lists, three sets trended toward down-regulation in DA-exposed animals (neuronal health, excitotoxicity, inflammation), but they did not meet the FDR cutoff of 0.25 (Table 4). The myelin, axons, and white matter set was found to be significantly up-regulated in DA-exposed animals ($q < 0.25$). This suggests that the set of genes in the myelin, axons, and white matter list were overly represented in the highest FC ranking of all transcripts examined (Figure 10A). Localized LFB staining for myelin indicated no histological evidence for hypomyelination (Figure 10B). Of the genes in this list, five were expressed with a log-FC ≥ 1.5 and $p \leq 0.05$ (Figure 10C), including kallikrein related peptidase 6 (*KLK6*), myelin associated glycoprotein (*MAG*), galactose-3-O-sulfotransferase 1 (*GAL3ST1*), and myelin and lymphocyte protein (*MAL*). Conversely, a down-regulation was observed for neuregulin 1 (*NRG1*).

Discussion

Although the excitotoxic properties of acute DA exposure have been well established in the nonhuman primate model,[16,17,81–87] lower levels of exposures had not been associated with signs of toxicity[38] until more recently.[39,43,52,88] Now, subtle effects resulting from prolonged exposures are of increasing concern.[89,90] Using exposures equivalent to the human regulatory limit[20–23] and

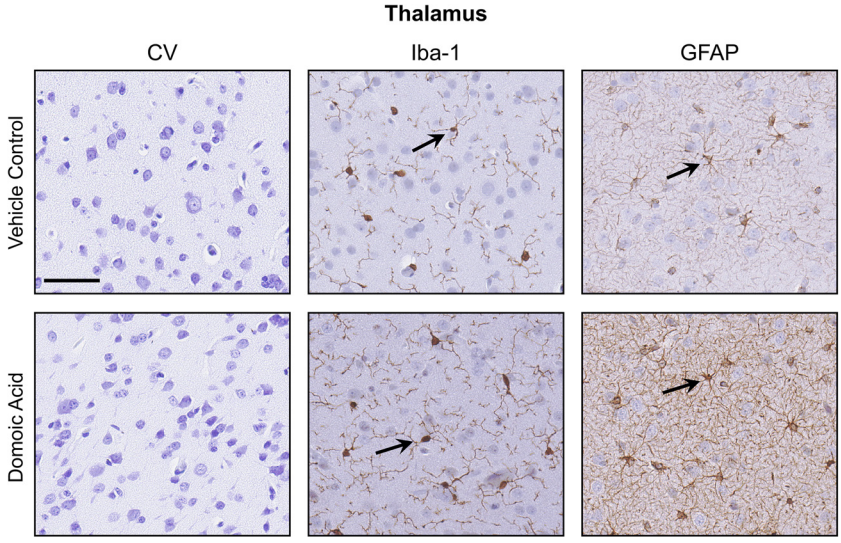

Figure 6. Differences in glial morphology in the thalamus. Representative images of staining of 10% formalin-fixed, paraffin-embedded, 10-µm sections of the thalamus for cresyl violet (CV) and immunohistochemistry ionized calcium binding adaptor molecule 1 (Iba-1; 1:2,000; Wako Chemicals) microglia; and glial fibrillary acidic protein (GFAP; 1:7,000, Dakocytomation) astrocytes from female *Macaca fascicularis* following prolonged exposed to domoic acid (0.15-mg/kg BW per day) or vehicle (5% sucrose). Immunoreactivity was visualized with Vectastain Elite and sections were counterstained with CV. CV staining showed no evidence of differences in the distribution of Nissl substance. Representative immunoreactive cells for Iba-1 or GFAP display as darker stained cells. Scale bar: 100 µm.

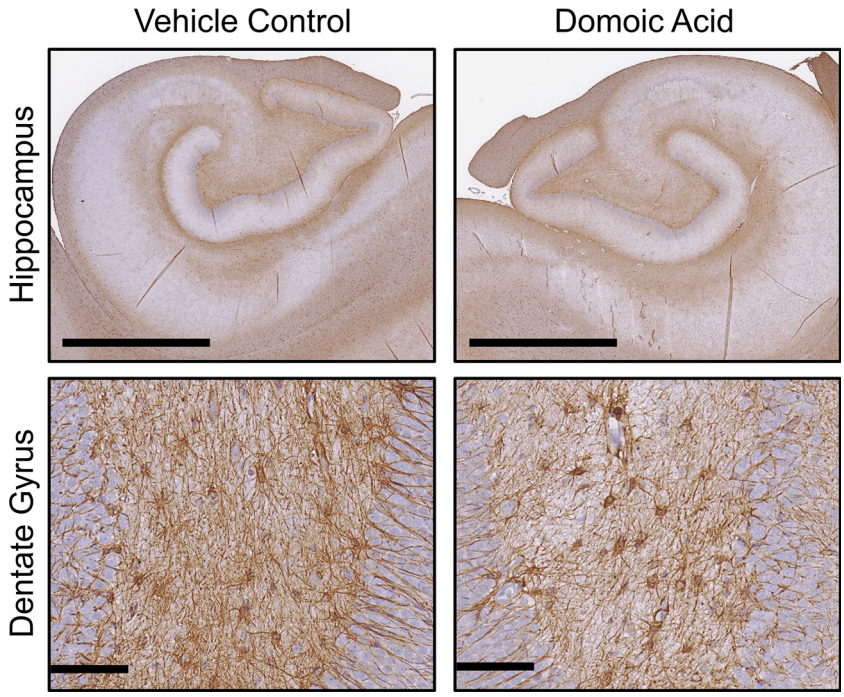

Figure 7. Immunohistochemistry for GFAP$^+$astrocytes in the hippocampus. Representative images of immunostaining of 10% formalin-fixed, paraffin-embedded, 10-µm sections for GFAP$^+$astrocytes (1:7,000; Dakocytomation) in the hippocampus of female *Macaca fascicularis* following prolonged exposed to domoic acid (0.15-mg/kg BW per day) or vehicle (5% sucrose). Images represent the hippocampus (scale bar: 2,000 µm) and the dentate gyrus (scale bar: 100 µm). Note: GFAP, glial fibrillary acidic protein.

contemporary human exposures,[28] previous experimental work with macaques found unexpected clinical effects manifesting as increased intention tremors after prolonged, daily exposure to DA.[39] Additional work with this cohort suggested that there were also subtle differences in in myelin tract integrity that were related to tremor frequency[43] and differences in the electrophysiology[52] of exposed animals. In the present study, the overall pattern obtained from the data from blood chemistry and cytokine levels suggested a lack of any overt systemic damage after low-level prolonged DA exposure. Yet data obtained by histological examination and RNAseq suggested a possible adaptative response in the brain to combat the subtle effects from DA. Thus, it is likely that the mild differences observed were a manifestation of compensatory responses or survival modalities against neurodegeneration.

Myelinated axons in the CNS are the "highways" of communication across cortical and subcortical regions, and healthy myelin sheathes facilitate this communication. The importance of myelin integrity is evident in various types of brain insults, multiple sclerosis, and age-related functional cognitive decline.[91] White matter FA is a measure from DTI that is related to structural integrity and, in humans, is often used as an index of white matter health.[92] Earlier work with the current cohort of monkeys assessed the whole-brain relationship to the DA-related tremors and suggested a negative correlation between tremors and voxel-wise FA in the

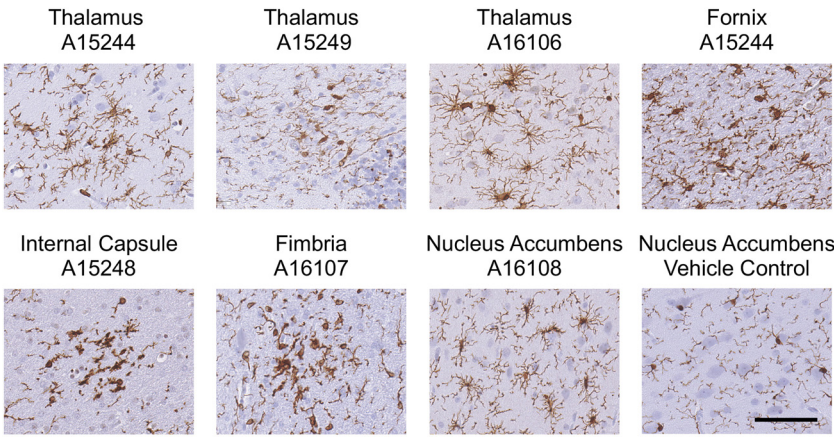

Figure 8. Focal sites of microglia reactivity. Representative images of Iba-1 immunopositive microglia in 10% formalin-fixed, paraffin-embedded, 10-µm sections at focal sites of reactivity in the thalamus, fornix, fimbria, internal capsule, and nucleus accumbens of female *Macaca fascicularis* following prolonged exposed to domoic acid (0.15-mg/kg BW per day) or vehicle (5% sucrose). Representative image of the nucleus accumbens in vehicle control is included for comparison. Representative images for the vehicle control fornix, fimbria, internal capsule, and thalamus are provided in Figures 4 and 6. Numbers correspond to Animal Numbers in Table S1. A15244 and A16106 were in the 0.15-mg/kg BW per day group; A15249, A16107, and A16106 were in the 0.075-mg/kg BW per day group; and A15428 was in the control group. Microglia were immunostained with antibody to Iba-1 (1:2,000; Wako Chemicals) followed by IgG antibody, visualized with Vectastain Elite (brown), and counterstained with cresyl violet (CV). Scale bar: 100 µm.

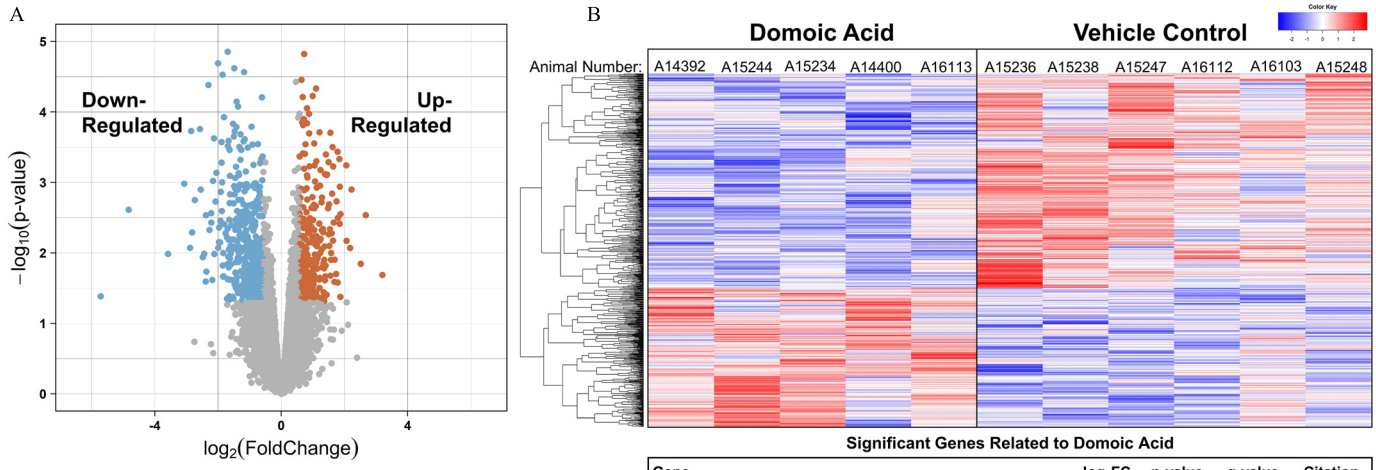

C

Highly Significant Genes (FDR q<0.05)

Gene	log_2FC	q-value
Chitinase 3 Like 1 (*CHI3L1*)	1.35	0.003
Early Growth Response 1 (*EGR1*)	1.10	0.046
Phospholipid Phosphatase 2 (*PLPP2*)	0.73	0.027
CDC42 Effector Protein 1 (*CDC42EP1*)	0.64	0.046
Phytanoyl-CoA Dioxygenase Domain Containing 1 (*PHYHD1*)	-1.25	0.008
Integrin Subunit Beta Like 1 (*ITGBL1*)	-1.31	0.014
Transmembrane Protein 100 (*TMEM100*)	-1.18	0.037
Dopamine Receptor D2 (*DRD2*)	-1.86	0.037
Vestigial Like Family Member 3 (*VGLL3*)	-4.39	0.006

D

Significant Genes Related to Domoic Acid

Gene	log_2FC	p-value	q-value	Citation
Activity-Regulated Cytoskeleton-Associated Protein (*ARC*)	0.83	0.001	0.16	1, 3
Fos Proto-Oncogene (*FOS*)	**1.12**	**0.001**	**0.18**	**1**
Early Growth Response 1 (*EGR1*)	1.10	<0.001	0.05	1, 2
Early Growth Response 2 (*EGR2*)	0.95	0.004	0.28	1
Early Growth Response 4 (*EGR4*)	**0.60**	**0.022**	**0.56**	**1**
Nuclear Receptor Subfamily 4 Group A Member (*NR4A1*)	1.07	0.001	0.17	1
BCL2 Interacting Protein 2 (*BNIP2*)	-0.68	0.02	0.50	2
Regulator of G Protein Signaling 9 (*RGS9*)	**-1.89**	**<0.001**	**0.10**	**2**
Ras-Related Protein - *RAB17**	1.20	0.02	0.58	2
Ras-Related Protein - *RAB44**	0.82	0.05	0.74	2
Dual Specificity Phosphatase 2 (*DUSP2*)	1.05	0.001	0.13	2, 3
Myocyte-Specific Enhancer Factor 2C (*MEF2C*)	0.70	0.01	0.43	3
Plakophilin 3 (*PKP3*)	1.48	0.002	0.23	3
Retinoid Isomerohydrolase - *RPE65*	-1.46	0.001	0.16	3

Figure 9. RNAseq transcriptional profiling of the hippocampus from female *Macaca fascicularis* following prolonged exposed to domoic acid (DA) or vehicle (5% sucrose). (A) Volcano plot shows differential expression between DA-exposed and unexposed groups. Each dot represents one gene. As indicated by the text, significantly down-regulated genes are highlighted on the left side and up-regulated gene are highlighted on the right side (log_2-FC >1.5 and $p \leq 0.05$). Genes along the middle indicate that expression was not significantly changed. (B) Heatmap shows significantly differentially expressed genes in both the exposed animals (left) and control animals (right). Each column represents an individual animal. A14392, A15244, and A15234 were in the 0.15-mg/kg BW per day group, and A14400 and A16113 were in the 0.075-mg/kg BW per day group. Blue highlighting indicates lower expression level and is observed in the upper two-thirds of the distribution for DA-exposed animals as compared with the lower one-third of the vehicle control animals. The red indicates high expression level and is an inverse distribution to those genes showing lower expression levels. The key in the upper right corner of the image provides the density gradient for the blue (lower) and red (upper). (C) Significant genes with a false discovery rate (FDR) of <0.05. All genes in this table had a $p < 0.001$. (D) Significant genes previously reported to be differentially expressed in either *a*) mice,[74] *b*) acute zebrafish,[75] or *c*) chronic zebrafish[76] after DA exposures. Bolded values indicate genes that were differentially expressed in the same direction across the previous studies. *Denotes unspecified homologous RAB gene identified in zebrafish. Note: FC, fold change; RNAseq, RNA sequencing.

fornix and internal capsule (major white matter tracts connecting the hippocampus and thalamus to other parts of the brain).[43] Low FA scores are indicative of either direct damage to the myelin/axonal tracts or the replacement of axonal bundles with other cells (i.e., glia).[93,94] The absence of differences currently observed with region-specific tractography and LFB staining for myelin suggests that the whole-brain differences in white matter integrity were not reflective of overt demyelination/hypomyelination. Instead, previously reported whole-brain FA differences may be related to an alternative mechanism, such as an inflammatory response or a response of the axon itself.[95]

An adaptive process in the myelin can also represent a form of neural plasticity, with ongoing activity-dependent changes to myelin, which may be influenced by the underlying axon.[96] RNAseq analyses from the hippocampus suggested an overall up-regulation of genes related to white matter, myelin, and axons, but whether this represented differences within the myelin sheath or the underlying axon is not known, especially given that genes for structural myelin proteins were similar between control and exposed animals. This evidence does, however, provide additional support for the earlier finding in these monkeys of an altered white matter integrity on MR imaging.[43] Myelination can

Table 4. Gene set enrichment results.

Gene set	Number of genes in set	Enrichment score	Normalized enrichment score	Normalized *p*-value	FDR
Up-regulated					
Myelin and white matter	33	0.65	2.06	<0.001*	<0.001*
Down-regulated					
Neuronal health	17	−0.46	−1.12	0.46	0.68
Excitotoxicity	57	−0.42	−1.23	0.50	0.45
Inflammation and glia	27	−0.36	−0.96	0.52	0.89

Note: Results from Gene Set Enrichment Analysis (GSEA) using four gene sets (listed in Table S2). Enrichment score reflects degree to which a defined gene set is overrepresented at the top or the bottom of total ranked data set of transcripts. Normalized enrichment score accounts for differences in the size of gene set and can be used to compare across gene sets of interest.[78,79] Significantly enriched set is denoted by an asterisk. FDR, false discovery rate.

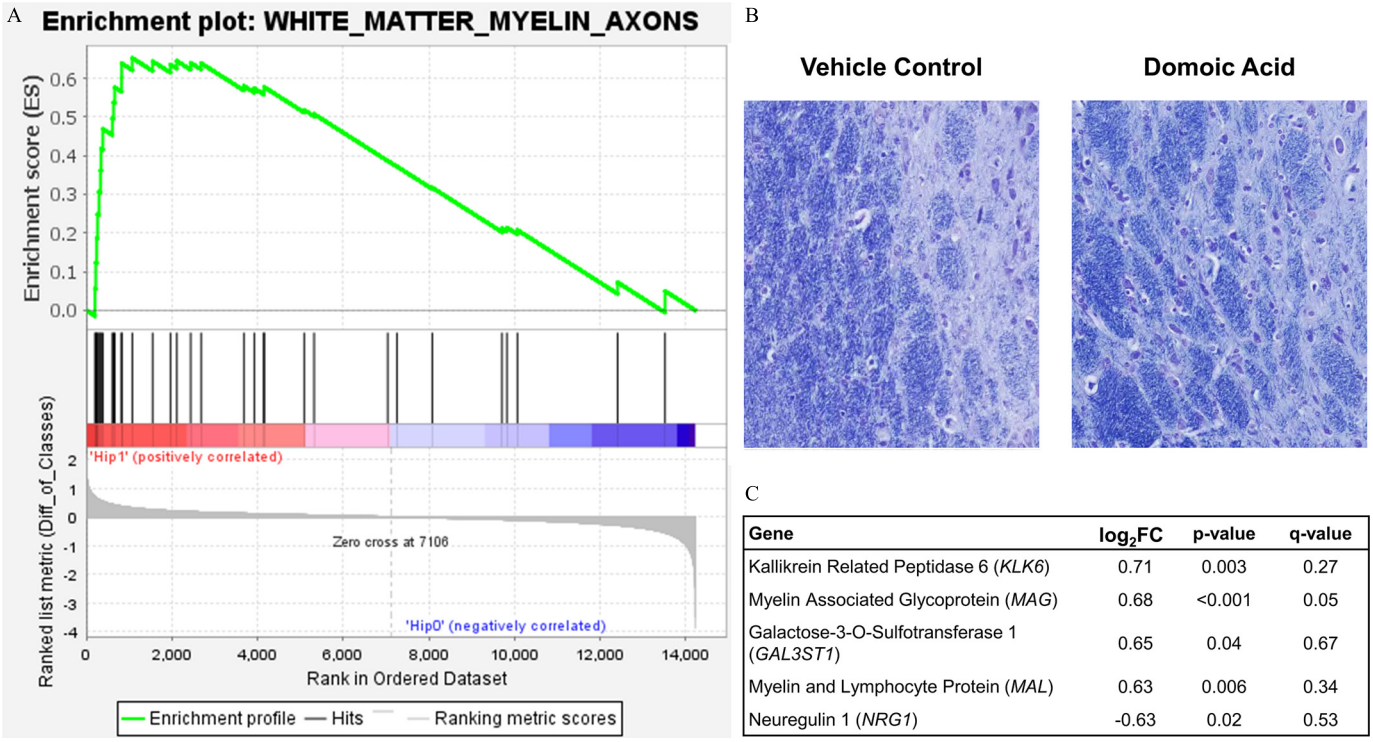

C

Gene	log_2FC	p-value	q-value
Kallikrein Related Peptidase 6 (*KLK6*)	0.71	0.003	0.27
Myelin Associated Glycoprotein (*MAG*)	0.68	<0.001	0.05
Galactose-3-O-Sulfotransferase 1 (*GAL3ST1*)	0.65	0.04	0.67
Myelin and Lymphocyte Protein (*MAL*)	0.63	0.006	0.34
Neuregulin 1 (*NRG1*)	-0.63	0.02	0.53

Figure 10. White matter response to domoic acid. (A) Gene Set Enrichment Analysis (GSEA) plot. The enrichment profile across all genes in that set from GSEA is shown in the upper panel curve, with the significant genes demarked underneath by black vertical lines and a scale representing genes up-regulated on the left (red) to those down-regulated on the right side (blue) of the panel. (B) Representation image of Luxol fast blue (LFB) staining for myelin in the hippocampus of vehicle control and domoic acid-exposed animals. (C) Significantly differentially expressed genes from the white matter GSEA list by log_2 FC. Note: Diff, difference; FC, fold change.

also be influenced by glutamate signaling,[95] the known toxic mechanism of acute DA toxicity, but the molecular profile of the hippocampus was largely absent of DEGs related to glutamate signaling. Yet, the single significant gene in the myelin network that was down-regulated, *NRG1*, acts as a switch for myelination processes that are either glutamate signaling dependent or independent,[97] providing a possible cell–cell communication link between the known mechanisms of action of DA and myelin stability. It is possible that, as a hallmark of prolonged low-level DA neurotoxicity, differences in myelin integrity could reflect multiple adaptations across the brain that contribute to the cognitive decline observed in humans commonly exposed to low levels of DA.[24–27] Results from other models have also noted white matter effects; white matter differences have been observed with developmental DA exposure in zebrafish[98] and with naturally exposed feral sea lions experiencing memory difficulties.[99,100] As the field gains a better understanding of the process of adaptive myelination and neural function, applying this knowledge to assess adverse health effects in the human population may bolster knowledge for effective preventative or intervention strategies.

Although there was a tacit assumption that the neurotoxic effects of DA would be related to its glutamatergic excitotoxic properties, we observed no histological evidence of an excitotoxicity-associated neuronal death or microglia response. Except for a single gene (*GRIN2B*), expression of genes related to glutamate receptors and signaling were also largely the same between controls and DA-exposed animals. The molecular response did, however, suggest DA-related differences in the expression of genes that are connected to regulatory functions and cell proliferation, rather than cellular degeneration. For example, many of the top up-regulated DEGs identified play important roles in tissue remodeling (*CHI3L1*), cytoskeletal function (*CDC42EP1*), and phospholipid production (*PLPP2*). In addition, the up-regulation of immediate early genes (e.g., *FOS* and EGR families) can be reflective of a rapid response to address mechanisms associated with brain plasticity and memory formation, as well as injury response.[101–103] Immediate early genes have also been implicated in acute responses to DA in both rodent models[74–76,85,87,104,105] and nonhuman primates.[84] In the present study, *FOS, FOSB, EGR1, EGR2,* and *EGR4* were significantly higher in the hippocampus when comparing DA-exposed to control animals, which may reflect neural efforts to regulate multiple processes in the brain that are normally not associated with DA-induced excitotoxicity. Alternatively or concurrently, they may reflect the adaptative changes in astrocytes that occurred with chronic, low-level DA exposure. Accordingly, three of the statistically significant genes ($p < 0.05$) found in DA-exposed animals that were related to astrocytes, including *ADORA2A, IGF2, and IGFBP5,* are associated with astrocyte interactions with microglia[106] and neurons,[107] as well as the regulation of IGF receptor signaling.

Astrocytes help regulate local interactions with multiple CNS components, including synapses, blood vessels, and other glial cells.[108] These cells express a wide repertoire of receptors, transporters, and other molecules that are essential for metabolic and homeostatic functions and synaptic regulation.[109,110] Their involvement in brain state transitions occurs through the release of gliotransmitters and regulation of extracellular potassium influencing the neuromodulatory networks.[111] Astrocytes are morphologically complex cells displaying an intricate arborization that is sensitive to the environment.[112–114] In response to injury or other environmental assaults, astrocytes often undergo a rapid and often reversible structural remodeling response, but the full astrocyte hypertrophy that typically accompanies robust neuronal death is not required for a functional astrocyte response.[115] Over the course of aging, the human brain has demonstrated an increased density of astrocyte cell

bodies, similar to what was observed in the present study, suggesting a biological response.[70]

For DA exposure, the patterns of astrocyte reactivity in primates[87] and rodents[32,116,117] have been primarily characterized by elevated levels of GFAP immunoreactivity and shifts in cell morphology that are reflective of hypertrophy, but a nonhypertrophic response in the monkey hippocampus has also been reported, occurring 6 months after a single, IV injection of DA (0.055 mg DA/kg BW).[118] In that instance, astrocytes from DA-exposed animals displayed a different GFAP staining pattern that showed evidence of inducing an acute CNS injury. This pattern was remarkably similar to that observed in the present study. These astrocytic responses, in absence of cooccurring neuronal death, may reflect a prolonged response to an earlier event. Alternatively, the pattern observed in the present study may represent a gradual morphological transformation without frank astrogliosis, as has been observed in normal human aging.[70] It is not known, however, if the morphological characteristics of the astrocytes represent a residual response that was initiated early in the exposure paradigm or, alternatively, a response that develops over time. In other models of prolonged exposure, weekly exposure for 22 wk in mice (0.75 mg DA/kg intraperitoneally) and for >36 wk in zebrafish (0.31 mg DA/g once a week for 6 wk, then 0.18 mg DA/g once every other week for 30 wk) did not result in any changes in neurons or $GFAP^{+}$astrocytes.[38,73] Other molecular and protein level changes were documented in these studies, namely, increases in the glutamate transporter, VGluT1, in synaptic boutons in the mice[38] and altered transcriptomic profile and mitochondrial function in zebrafish brains.[73] In the monkey, prolonged, low-dose DA exposure may represent a subthreshold level of glutamatergic signaling that is insufficient for neuronal excitotoxicity but adequate to stimulate a response from astrocytes. This response could be either directly caused by glutamate or, more so, an interaction with the neurons.

Although the primary site of damage with an excitotoxin is the hippocampus, an involvement of the thalamus has also been implicated in acute DA neurotoxicity in nonhuman primates[86] and rats.[32,119,120] In the present study, no evidence of neuronal death or related astrocyte hypertrophy or microglia activation was observed in the thalamus. Instead, we observed a distinct difference of DA-exposed microglia morphology characterized by larger soma size and extended processes that, when combined with the absence of an acute injury phenotype, may represent cell–cell interactions required for maintaining regulatory functions and neuronal survival.[121–123] Alternatively, this may represent direct actions of DA on microglia.[34,35,124,125] Although the thalamus was not a focus for molecular profiling, the subtle differences observed in microglia and astrocytes suggested that identifying DEGs in the thalamus would be beneficial in determining the underlying nature of the response and possibly identifying compensatory gene responses.

Multifocal microscopic hemorrhages absent of cellular necrosis or apoptosis have been observed in sea otter brains after natural exposure to DA,[126] and the authors suggested that these were indicative of previously active damage in response to subacute or chronic exposure to DA. In the present study, focal sites of injury (cluster reactions of microglia) were observed across multiple DA-exposed animals, in the thalamus, fornix, fimbria, and nucleus accumbens. These reactions likely represented an *a priori* event; they appeared without colocalized cell death or astrocyte hypertrophy and without indications of congestion or meningeal hemorrhage. In cases of mild hemorrhagic or neurovascular injury, prolonged microglia activation contributes to performing a clearance and repair task.[127–129] Although imaging for the neurovasculature was not conducted, there was no indication of infiltrating blood-borne cells. Thus, the focal microglia responses observed could have been in response to prior relatively minor and short-lived vascular insults.

Human Health Implications

Current regulatory limits for DA were designed to protect adults against overt toxicity associated with acute, high-dose exposures. Since 1987, they have been successful in preventing cases of human acute poisonings.[130] Yet with changing climatic patterns that have triggered longer-lasting DA–algal blooms,[131,132] there is an increasing chance that repeated DA exposure may occur at closer and closer intervals, resulting in a greater level of human exposure. Accordingly, the public health concern has shifted focus to protecting vulnerable populations who are exposed to low levels of DA for prolonged periods of time (some for a lifetime). Given the environmentally relevant exposure levels and route of exposure used in the present study, the findings suggested that subacutely toxic levels of DA exposure were not absent of neurological effects but, rather, were sufficient to induce the system to respond to the low-level insult. The chronic nature of this activation may alter the ability of the nervous system to respond to subsequent insults, potentially shifting the underlying risk for other age-related health effects, such as neurodegenerative and neurovasculature disorders. Future regulatory guidance on DA should consider these findings and the fact that even smaller shifts in cell activation or response can impact future responses to environmental exposures and diseases. The long-term consequences of such shifts should be taken into consideration and addressed with regard to the health risks of affected populations, especially coastal Native American and Indigenous populations who have not been traditionally included in the policy development and regulation regarding this common marine toxin.

Acknowledgments

We acknowledge and thank the dedicated staff and volunteers of the Infant Primate Research Laboratory and the University of Washington National Primate Research Center for their skilled assistance in this research; T. Wilbur for this help with the radiofrequency coil and magnetic resonance scanning; S. Ellis for data assistance; the staff at the University of Washington Diagnostics Imaging Sciences Center for their technical aid; and the National Institute of Environmental Health Sciences histology core for their support in the histopathology processing. Research from this project was supported by U.S. National Institutes of Health [NIH; R01 ES023043 (T.M.B.), P51 OD010425, HD083091, T32ES007062 (R.L.P.)], P30ES007033, and the NIH/National Center for Advancing Translational Sciences [TL1 TR000422 (S.S.)], and the NIH Intramural Research Program Z01 ES021164.

The RNA sequencing data have been deposited in the National Center for Biotechnology Information Gene Expression Omnibus with the accession number GSE163026.

References

1. Bates SS, Hubbard KA, Lundholm N, Montresor M, Leaw CP. 2018. *Pseudo-nitzschia, Nitzschia*, and domoic acid: new research since 2011. Harmful Algae 79:3–43, PMID: 30420013, https://doi.org/10.1016/j.hal.2018.06.001.
2. Brunson JK, McKinnie SMK, Chekan JR, McCrow JP, Miles ZD, Bertrand EM, et al. 2018. Biosynthesis of the neurotoxin domoic acid in a bloom-forming diatom. Science 361(6409):1356–1358, PMID: 30262498, https://doi.org/10.1126/science.aau0382.
3. Zaman L, Arakawa O, Shimosu A, Onoue Y, Nishio S, Shida Y, et al. 1997. Two new isomers of domoic acid from a red alga, *Chondria armata*. Toxicon 35(2):205–212, PMID: 9080577, https://doi.org/10.1016/S0041-0101(96)00123-7.

4. Steele TS, Brunson JK, Maeno Y, Terada R, Allen AE, Yotsu-Yamashita M, et al. 2022. Domoic acid biosynthesis in the red alga *Chondria armata* suggests a complex evolutionary history for toxin production. Proc Natl Acad Sci USA 119(6):e2117407119, PMID: 35110408, https://doi.org/10.1073/pnas.2117407119.
5. Trainer VL, Bates SS, Lundholm N, Thessen AE, Cochlan WP, Adams NG, et al. 2012. *Pseudo-nitzschia* physiological ecology, phylogeny, toxicity, monitoring and impacts on ecosystem health. Harmful Algae 14:271–300, https://doi.org/10.1016/j.hal.2011.10.025.
6. Greig DJ, Gulland FMD, Kreuder C. 2010. A decade of live California sea lion (Zalophus californianus) strandings along the central California Coast: causes and trends, 1991–2000. Aquatic Mammals 31(1):11–22, https://doi.org/10.1578/AM.31.1.2005.11.
7. Lefebvre KA, Quakenbush L, Frame E, Huntington KB, Sheffield G, Stimmelmayr R, et al. 2016. Prevalence of algal toxins in Alaskan marine mammals foraging in a changing arctic and subarctic environment. Harmful Algae 55:13–24, PMID: 28073526, https://doi.org/10.1016/j.hal.2016.01.007.
8. Perl TM, Bédard L, Kosatsky T, Hockin JC, Todd EC, Remis RS. 1990. An outbreak of toxic encephalopathy caused by eating mussels contaminated with domoic acid. N Engl J Med 322(25):1775–1780, PMID: 1971709, https://doi.org/10.1056/NEJM199006213222504.
9. Jeffery B, Barlow T, Moizer K, Paul S, Boyle C. 2004. Amnesic shellfish poison. Food Chem Toxicol 42(4):545–557, PMID: 15019178, https://doi.org/10.1016/j.fct.2003.11.010.
10. Teitelbaum JS, Zatorre RJ, Carpenter S, Gendron D, Evans AC, Gjedde A, et al. 1990. Neurologic sequelae of domoic acid intoxication due to the ingestion of contaminated mussels. N Engl J Med 322(25):1781–1787, PMID: 1971710, https://doi.org/10.1056/NEJM199006213222505.
11. Cendes F, Andermann F, Carpenter S, Zatorre RJ, Cashman NR. 1995. Temporal lobe epilepsy caused by domoic acid intoxication: evidence for glutamate receptor-mediated excitotoxicity in humans. Ann Neurol 37(1):123–126, PMID: 7818246, https://doi.org/10.1002/ana.410370125.
12. Goldstein T, Mazet JAK, Zabka TS, Langlois G, Colegrove KM, Silver M, et al. 2008. Novel symptomatology and changing epidemiology of domoic acid toxicosis in California sea lions (*Zalophus californianus*): an increasing risk to marine mammal health. Proc Biol Sci 275(1632):267–276, PMID: 18006409, https://doi.org/10.1098/rspb.2007.1221.
13. Silvagni PA, Lowenstine LJ, Spraker T, Lipscomb TP, Gulland FMD. 2005. Pathology of domoic acid toxicity in California sea lions (*Zalophus californianus*). Vet Pathol 42(2):184–191, PMID: 15753472, https://doi.org/10.1354/vp.42-2-184.
14. Buckmaster PS, Wen X, Toyoda I, Gulland FMD, Van Bonn W. 2014. Hippocampal neuropathology of domoic acid-induced epilepsy in California sea lions (*Zalophus californianus*). J Comp Neurol 522(7):1691–1706, PMID: 24638960, https://doi.org/10.1002/cne.23509.
15. Iverson F, Truelove J, Nera E, Tryphonas L, Campbell J, Lok E. 1989. Domoic acid poisoning and mussel-associated intoxication: preliminary investigations into the response of mice and rats to toxic mussel extract. Food Chem Toxicol 27(6):377–384, PMID: 2792967, https://doi.org/10.1016/0278-6915(89)90143-9.
16. Iverson F, Truelove J, Tryphonas L, Nera EA. 1990. The toxicology of domoic acid administered systemically to rodents and primates. Can Dis Wkly Rep 16(suppl 1E):15–18, PMID: 2101735.
17. Tryphonas L, Truelove J, Iverson F. 1990. Acute parenteral neurotoxicity of domoic acid in cynomolgus monkeys (M. fascicularis). Toxicol Pathol 18(2):297–303, PMID: 2268382, https://doi.org/10.1177/019262339001800208.
18. Tryphonas L, Truelove J, Nera E, Iverson F. 1990. Acute neurotoxicity of domoic acid in the rat. Toxicol Pathol 18(1 pt 1):1–9, PMID: 2362984, https://doi.org/10.1177/019262339001800101.
19. FDA (U.S. Food and Drug Administration). 2021. Chapter 6: Natural toxins. In: *Fish and Fishery Products Hazards and Controls Guidance*. 4th ed. Washington, DC: Department of Health and Human Services.
20. Toyofuku H. 2006. Joint FAO/WHO/IOC activities to provide scientific advice on marine biotoxins. Mar Pollut Bull 52(12):1735–1745, PMID: 16979668, https://doi.org/10.1016/j.marpolbul.2006.07.007.
21. Lawrence J, Loreal H, Toyofuku H, Hess P, Iddya K, Ababouch L. 2011. *Assessment and Management of Biotoxin Risks in Bivalve Molluscs*. FAO Fisheries and Aquaculture Technical Paper 551. Rome, Italy: Food and Agriculture Organization of the United Nations (FAO). https://www.fao.org/docrep/015/i2356e/i2356e.pdf [accessed 20 May 2022].
22. Wekell JC, Hurst J, Lefebvre KA. 2004. The origin of the regulatory limits for PSP and ASP toxins in shellfish. J Shellfish Res 23(3):927–930.
23. Mariën K. 1996. Establishing tolerable dungeness crab (*Cancer magister*) and razor clam (*Siliqua patula*) domoic acid contaminant levels. Environ Health Perspect 104(11):1230–1236, PMID: 8959413, https://doi.org/10.1289/ehp.104-1469507.
24. Grattan LM, Boushey C, Tracy K, Trainer VL, Roberts SM, Schluterman N, et al. 2016. The association between razor clam consumption and memory in the CoASTAL cohort. Harmful Algae 57(B):20–25, PMID: 27746706, https://doi.org/10.1016/j.hal.2016.03.011.
25. Grattan LM, Boushey CJ, Liang Y, Lefebvre KA, Castellon LJ, Roberts KA, Toben AC, et al. 2018. Repeated dietary exposure to low levels of domoic acid and problems with everyday memory: research to public health outreach. Toxins (Basel) 10(3):103, PMID: 29495583, https://doi.org/10.3390/toxins10030103.
26. Stuchal LD, Grattan LM, Portier KM, Kilmon KA, Manahan LM, Roberts SM, et al. 2020. Dose-response assessment for impaired memory from chronic exposure to domoic acid among Native American consumers of razor clams. Regul Toxicol Pharmacol 117:104759, PMID: 32768666, https://doi.org/10.1016/j.yrtph.2020.104759.
27. Grattan LM, Kaddis L, Tracy JK, Morris JG. 2021. Long term memory outcome of repetitive, low-level dietary exposure to domoic acid in Native Americans. Int J Environ Res Public Health 18(8):3955, PMID: 33918677, https://doi.org/10.3390/ijerph18083955.
28. Ferriss BE, Marcinek DJ, Ayres D, Borchert J, Lefebvre KA. 2017. Acute and chronic dietary exposure to domoic acid in recreational harvesters: a survey of shellfish consumption behavior. Environ Int 101:70–79, PMID: 28109640, https://doi.org/10.1016/j.envint.2017.01.006.
29. Tracy K, Boushey CJ, Roberts SM, Morris JG Jr, Grattan LM. 2016. Communities advancing the studies of tribal nations across their lifespan: design, methods, and baseline of the CoASTAL cohort. Harmful Algae 57(B):9–19, PMID: 27616972, https://doi.org/10.1016/j.hal.2016.03.010.
30. Trainer VL, Moore SK, Hallegraeff G, Kudela RM, Clement A, Mardones JI, et al. 2020. Pelagic harmful algal blooms and climate change: lessons from nature's experiments with extremes. Harmful Algae 91:101591, PMID: 32057339, https://doi.org/10.1016/j.hal.2019.03.009.
31. Berdalet E, Fleming LE, Gowen R, Davidson K, Hess P, Backer LC, et al. 2015. Marine harmful algal blooms, human health and wellbeing: challenges and opportunities in the 21st century. J Mar Biol Assoc UK 96(1):61–91, PMID: 26692586, https://doi.org/10.1017/S0025315415001733.
32. Vieira AC, Alemañ N, Cifuentes JM, Bermúdez R, López Peña M, Botana LM. 2015. Brain pathology in adult rats treated with domoic acid. Vet Pathol 52(6):1077–1086, PMID: 25939577, https://doi.org/10.1177/0300985815584074.
33. Chandrasekaran A, Ponnambalam G, Kaur C. 2004. Domoic acid-induced neurotoxicity in the hippocampus of adult rats. Neurotox Res 6(2):105–117, PMID: 15325963, https://doi.org/10.1007/BF03033213.
34. Ananth C, Gopalakrishnakone P, Kaur C. 2003. Induction of inducible nitric oxide synthase expression in activated microglia following domoic acid (DA)-induced neurotoxicity in the rat hippocampus. Neurosci Lett 338(1):49–52, PMID: 12565138, https://doi.org/10.1016/s0304-3940(02)01351-4.
35. Ananth C, Thameem Dheen S, Gopalakrishnakone P, Kaur C. 2001. Domoic acid-induced neuronal damage in the rat hippocampus: changes in apoptosis related genes (bcl-2, bax, caspase-3) and microglial response. J Neurosci Res 66(2):177–190, PMID: 11592113, https://doi.org/10.1002/jnr.1210.
36. Lefebvre KA, Kendrick PS, Ladiges W, Hiolski EM, Ferriss BE, Smith DR, et al. 2017. Chronic low-level exposure to the common seafood toxin domoic acid causes cognitive deficits in mice. Harmful Algae 64:20–29, PMID: 28427569, https://doi.org/10.1016/j.hal.2017.03.003.
37. Moyer CE, Hiolski EM, Marcinek DJ, Lefebvre KA, Smith DR, Zuo Y. 2018. Repeated low level domoic acid exposure increases CA1 VGluT1 levels, but not bouton density, VGluT2 or VGAT levels in the hippocampus of adult mice. Harmful Algae 79:74–86, PMID: 30420019, https://doi.org/10.1016/j.hal.2018.08.008.
38. Truelove J, Mueller R, Pulido O, Martin L, Fernie S, Iverson F. 1997. 30-day oral toxicity study of domoic acid in cynomolgus monkeys: lack of overt toxicity at doses approaching the acute toxic dose. Nat Toxins 5(3):111–114, PMID: 9285915, https://doi.org/10.1002/1522-7189(1997)5:3<111::AID-NT5>3.0.CO;2-6.
39. Burbacher TM, Grant KS, Petroff R, Shum S, Crouthamel B, Stanley C, et al. 2019. Effects of oral domoic acid exposure on maternal reproduction and infant birth characteristics in a preclinical nonhuman primate model. Neurotoxicol Teratol 72:10–21, PMID: 30615984, https://doi.org/10.1016/j.ntt.2019.01.001.
40. Mantini D, Hasson U, Betti V, Perrucci MG, Romani GL, Corbetta M, et al. 2012. Interspecies activity correlations reveal functional correspondence between monkey and human brain areas. Nat Methods 9(3):277–282, PMID: 22306809, https://doi.org/10.1038/nmeth.1868.
41. Miranda-Dominguez O, Mills BD, Grayson D, Woodall A, Grant KA, Kroenke CD, et al. 2014. Bridging the gap between the human and macaque connectome: a quantitative comparison of global interspecies structure–function relationships and network topology. J Neurosci 34(16):5552–5563, PMID: 24741045, https://doi.org/10.1523/JNEUROSCI.4229-13.2014.
42. Kumar PM, Kumar SP, Nair GA. 2009. Risk assessment of the amnesiac shellfish poison, domoic acid, on animals and humans. J Environ Biol 30(3):319–325, PMID: 20120452.
43. Petroff R, Richards T, Crouthamel B, McKain N, Stanley C, Grant KS, et al. 2019. Chronic, low-level oral exposure to marine toxin, domoic acid, alters whole brain morphometry in nonhuman primates. Neurotoxicology 72:114–124, PMID: 30826346, https://doi.org/10.1016/j.neuro.2019.02.016.

44. Hanig J, Paule MG, Ramu J, Schmued L, Konak T, Chigurupati S, et al. 2014. The use of MRI to assist the section selections for classical pathology assessment of neurotoxicity. Regul Toxicol Pharmacol 70(3):641–647, PMID: 25265367, https://doi.org/10.1016/j.yrtph.2014.09.010.
45. Zhang Y, Jonkman L, Klauser A, Barkhof F, Yong VW, Metz LM, et al. 2016. Multi-scale MRI spectrum detects differences in myelin integrity between MS lesion types. Mult Scler 22(12):1569–1577, PMID: 26754802, https://doi.org/10.1177/1352458515624771.
46. Jones NR, Blumbergs PC, Brown CJ, McLean AJ, Manavis J, Perrett LV, et al. 1998. Correlation of postmortem MRI and CT appearances with neuropathology in brain trauma: a comparison of two methods. J Clin Neurosci 5(1):73–79, PMID: 18644293, https://doi.org/10.1016/S0967-5868(98)90207-7.
47. Animal Welfare Act of 1970. Pub L No. 89–544, §1(a).
48. National Research Council. 2011. *Guide for the Care and Use of Laboratory Animals*. 8th ed. Washington, DC: National Academies Press.
49. Jing J, Petroff R, Shum S, Crouthamel B, Topletz AR, Grant KS, et al. 2018. Toxicokinetics and physiologically based pharmacokinetic modeling of the shellfish toxin domoic acid in nonhuman primates. Drug Metab Dispos 46(2):155–165, PMID: 29150543, https://doi.org/10.1124/dmd.117.078485.
50. Shum S, Kirkwood JS, Jing J, Petroff R, Crouthamel B, Grant KS, et al. 2018. Validated HPLC-MS/MS method to quantify low levels of domoic acid in plasma and urine after subacute exposure. ACS Omega 3(9):12079–12088, PMID: 30320288, https://doi.org/10.1021/acsomega.8b02115.
51. Shum S, Jing J, Petroff R, Crouthamel B, Grant KS, Burbacher TM, et al. 2020. Maternal-fetal disposition of domoic acid following repeated oral dosing during pregnancy in nonhuman primate. Toxicol Appl Pharmacol 398:115027, PMID: 32360744, https://doi.org/10.1016/j.taap.2020.115027.
52. Petroff R, Murias M, Grant KS, Crouthamel B, McKain N, Shum S, et al. 2020. Power spectrum analysis of EEG in a translational nonhuman primate model after chronic exposure to low levels of the common marine neurotoxin, domoic acid. Neurotoxicology 80:124–129, PMID: 32717199, https://doi.org/10.1016/j.neuro.2020.07.006.
53. Burbacher TM, Grant KS, Shen DD, Sheppard L, Damian D, Ellis S, et al. 2004. Chronic maternal methanol inhalation in nonhuman primates (*Macaca fascicularis*): reproductive performance and birth outcome. Neurotoxicol Teratol 26(5):639–650, PMID: 15315813, https://doi.org/10.1016/j.ntt.2004.06.001.
54. Burbacher T, Shen D, Grant K, Sheppard L, Damian D, Ellis S, et al. 1999. *Reproductive and Offspring Developmental Effects Following Maternal Inhalation Exposure to Methanol in Nonhuman Primates*. Research Report 89. Boston, MA: Health Effects Institute.
55. Jacobson Misbe EN, Richards TL, McPherson RJ, Burbacher TM, Juul SE. 2011. Perinatal asphyxia in a nonhuman primate model. Dev Neurosci 33(3–4):210–221, PMID: 21659720, https://doi.org/10.1159/000327246.
56. Andersson JLR, Skare S, Ashburner J. 2003. How to correct susceptibility distortions in spin-echo echo-planar images: application to diffusion tensor imaging. Neuroimage 20(2):870–888, PMID: 14568458, https://doi.org/10.1016/S1053-8119(03)00336-7.
57. Jenkinson M, Bannister P, Brady M, Smith S. 2002. Improved optimization for the robust and accurate linear registration and motion correction of brain images. Neuroimage 17(2):825–841, PMID: 12377157, https://doi.org/10.1016/s1053-8119(02)91132-8.
58. Jenkinson M, Smith S. 2001. A global optimisation method for robust affine registration of brain images. Med Image Anal 5(2):143–156, PMID: 11516708, https://doi.org/10.1016/S1361-8415(01)00036-6.
59. Jenkinson M, Beckmann CF, Behrens TEJ, Woolrich MW, Smith SM. 2012. FSL. Neuroimage 62(2):782–790, PMID: 21979382, https://doi.org/10.1016/j.neuroimage.2011.09.015.
60. Avants BB, Tustison NJ, Song G, Cook PA, Klein A, Gee JC. 2011. A reproducible evaluation of ANTs similarity metric performance in brain image registration. Neuroimage 54(3):2033–2044, PMID: 20851191, https://doi.org/10.1016/j.neuroimage.2010.09.025.
61. Rohlfing T, Kroenke CD, Sullivan EV, Dubach MF, Bowden DM, Grant KA, et al. 2012. The INIA19 template and Neuromaps Atlas for primate brain image parcellation and spatial normalization. Front Neuroinform 6:27, PMID: 23230398, https://doi.org/10.3389/fninf.2012.00027.
62. Smith SM, Jenkinson M, Woolrich MW, Beckmann CF, Behrens TEJ, Johansen-Berg H, et al. 2004. Advances in functional and structural MR image analysis and implementation as FSL. Neuroimage 23(suppl 1):S208–S219, PMID: 15501092, https://doi.org/10.1016/j.neuroimage.2004.07.051.
63. Behrens TEJ, Johansen Berg H, Jbabdi S, Rushworth MFS, Woolrich MW. 2007. Probabilistic diffusion tractography with multiple fibre orientations: what can we gain? Neuroimage 34(1):144–155, PMID: 17070705, https://doi.org/10.1016/j.neuroimage.2006.09.018.
64. Winkler AM, Ridgway GR, Webster MA, Smith SM, Nichols TE. 2014. Permutation inference for the general linear model. Neuroimage 92:381–397, PMID: 24530839, https://doi.org/10.1016/j.neuroimage.2014.01.060.
65. Smith SM, Nichols TE. 2009. Threshold-free cluster enhancement: addressing problems of smoothing, threshold dependence and localisation in cluster inference. Neuroimage 44(1):83–98, PMID: 18501637, https://doi.org/10.1016/j.neuroimage.2008.03.061.
66. Leary S, Underwood W, Anthony R, Cartner S, Grandin T, Greenacre C, et al. 2020. *AVMA Guidelines for the Euthanasia of Animals: 2020 edition*. Schaumburg, IL: American Veterinary Medical Association.
67. Kluver H, Barrera E. 1953. A method for the combined staining of cells and fibers in the nervous system. J Neuropathol Exp Neurol 12(4):400–403, PMID: 13097193, https://doi.org/10.1097/00005072-195312040-00008.
68. Oh SJ. 2001. *Color Atlas of Nerve Biopsy Pathology*. 1st ed. Hoboken, NJ: CRC Press.
69. Mikula S, Trotts I, Stone JM, Jones EG. 2007. Internet-enabled high-resolution brain mapping and virtual microscopy. Neuroimage 35(1):9–15, PMID: 17229579, https://doi.org/10.1016/j.neuroimage.2006.11.053.
70. Jyothi HJ, Vidyadhara DJ, Mahadevan A, Philip M, Parmar SK, Manohari SG, et al. 2015. Aging causes morphological alterations in astrocytes and microglia in human substantia nigra pars compacta. Neurobiol Aging 36(12):3321–3333, PMID: 26433682, https://doi.org/10.1016/j.neurobiolaging.2015.08.024.
71. Law CW, Chen Y, Shi W, Smyth GK. 2014. voom: precision weights unlock linear model analysis tools for RNA-seq read counts. Genome Biol 15(2):R29, PMID: 24485249, https://doi.org/10.1186/gb-2014-15-2-r29.
72. Smyth GK. 2004. Linear models and empirical Bayes methods for assessing differential expression in microarray experiments. Stat Appl Genet Mol Biol 3: Article3, PMID: 16646809, https://doi.org/10.2202/1544-6115.1027.
73. Phipson B, Lee S, Majewski IJ, Alexander WS, Smyth GK. 2016. Robust hyperparameter estimation protects against hypervariable genes and improves power to detect differential expression. Ann Appl Stat 10(2):946–963, PMID: 28367255, https://doi.org/10.1214/16-AOAS920.
74. Ryan JC, Morey JS, Ramsdell JS, Van Dolah FM. 2005. Acute phase gene expression in mice exposed to the marine neurotoxin domoic acid. Neuroscience 136(4):1121–1132, PMID: 16216424, https://doi.org/10.1016/j.neuroscience.2005.08.047.
75. Lefebvre KA, Tilton SC, Bammler TK, Beyer RP, Srinouanprachan S, Stapleton PL, et al. 2009. Gene expression profiles in zebrafish brain after acute exposure to domoic acid at symptomatic and asymptomatic doses. Toxicol Sci 107(1):65–77, PMID: 18936300, https://doi.org/10.1093/toxsci/kfn207.
76. Hiolski EM, Kendrick PS, Frame ER, Myers MS, Bammler TK, Beyer RP, et al. 2014. Chronic low-level domoic acid exposure alters gene transcription and impairs mitochondrial function in the CNS. Aquat Toxicol 155:151–159, PMID: 25033243, https://doi.org/10.1016/j.aquatox.2014.06.006.
77. Cahoy JD, Emery B, Kaushal A, Foo LC, Zamanian JL, Christopherson KS, et al. 2008. A transcriptome database for astrocytes, neurons, and oligodendrocytes: a new resource for understanding brain development and function. J Neurosci 28(1):264–278, PMID: 18171944, https://doi.org/10.1523/jneurosci.4178-07.2008.
78. Mootha VK, Lindgren CM, Eriksson KF, Subramanian A, Sihag S, Lehar J, et al. 2003. PGC-1α-responsive genes involved in oxidative phosphorylation are coordinately downregulated in human diabetes. Nat Genet 34(3):267–273, PMID: 12808457, https://doi.org/10.1038/ng1180.
79. Subramanian A, Tamayo P, Mootha VK, Mukherjee S, Ebert BL, Gillette MA, et al. 2005. Gene Set Enrichment Analysis: a knowledge-based approach for interpreting genome-wide expression profiles. Proc Natl Acad Sci USA 102(43):15545–15550, PMID: 16199517, https://doi.org/10.1073/pnas.0506580102.
80. Pappas DJ, Gabatto PA, Oksenberg D, Khankhanian P, Baranzini SE, Gan L, et al. 2012. Transcriptional expression patterns triggered by chemically distinct neuroprotective molecules. Neuroscience 226:10–20, PMID: 22986168, https://doi.org/10.1016/j.neuroscience.2012.09.007.
81. Truelove J, Iverson F. 1994. Serum domoic acid clearance and clinical observations in the cynomolgus monkey and Sprague-Dawley rat following a single i.v. dose. Bull Environ Contam Toxicol 52(4):479–486, PMID: 8167439, https://doi.org/10.1007/BF00194132.
82. Tryphonas L, Truelove J, Iverson F, Todd EC, Nera EA. 1990. Neuropathology of experimental domoic acid poisoning in non-human primates and rats. Can Dis Wkly Rep 16(suppl 1E):75–81, PMID: 2101744.
83. Tryphonas L, Truelove J, Todd E, Nera E, Iverson F. 1990. Experimental oral toxicity of domoic acid in cynomolgus monkeys (*Macaca fascicularis*) and rats. Preliminary investigations. Food Chem Toxicol 28(10):707–715, PMID: 2276699, https://doi.org/10.1016/0278-6915(90)90147-f.
84. Scallet AC, Binienda Z, Caputo FA, Hall S, Paule MG, Rountree RL, et al. 1993. Domoic acid-treated cynomolgus monkeys (*M. fascicularis*): effects of dose on hippocampal neuronal and terminal degeneration. Brain Res 627(2):307–313, PMID: 8298975, https://doi.org/10.1016/0006-8993(93)90335-k.
85. Scallet AC, Kowalke PK, Rountree RL, Thorn BT, Binienda ZK. 2004. Electroencephalographic, behavioral, and c-*fos* responses to acute domoic acid exposure. Neurotoxicol Teratol 26(2):331–342, PMID: 15019966, https://doi.org/10.1016/j.ntt.2003.10.004.

86. Schmued LC, Scallet AC, Slikker W Jr. 1995. Domoic acid-induced neuronal degeneration in the primate forebrain revealed by degeneration specific histochemistry. Brain Res 695(1):64–70, PMID: 8574649, https://doi.org/10.1016/0006-8993(95)00799-v.
87. Scallet AC, Schmued LC, Johannessen JN. 2005. Neurohistochemical biomarkers of the marine neurotoxicant, domoic acid. Neurotoxicol Teratol 27(5):745–752, PMID: 16203121, https://doi.org/10.1016/j.ntt.2005.06.018.
88. Grant KS, Crouthamel B, Kenney C, McKain N, Petroff R, Shum S, et al. 2019. Preclinical modeling of exposure to a global marine bio-contaminant: effects of in utero domoic acid exposure on neonatal behavior and infant memory. Neurotoxicol Teratol 73:1–8, PMID: 30690118, https://doi.org/10.1016/j.ntt.2019.01.003.
89. Grant KS, Burbacher TM, Faustman EM, Gratttan L. 2010. Domoic acid: neurobehavioral consequences of exposure to a prevalent marine biotoxin. Neurotoxicol Teratol 32(2):132–141, PMID: 19799996, https://doi.org/10.1016/j.ntt.2009.09.005.
90. Petroff R, Hendrix A, Shum S, Grant KS, Lefebvre KA, Burbacher TM. 2021. Public health risks associated with chronic, low-level domoic acid exposure: a review of the evidence. Pharmacol Ther 227:107865, PMID: 33930455, https://doi.org/10.1016/j.pharmthera.2021.107865.
91. Liu H, Yang Y, Xia Y, Zhu W, Leak RK, Wei Z, et al. 2017. Aging of cerebral white matter. Ageing Res Rev 34:64–76, PMID: 27865980, https://doi.org/10.1016/j.arr.2016.11.006.
92. Kochunov P, Thompson PM, Lancaster JL, Bartzokis G, Smith S, Coyle T, et al. 2007. Relationship between white matter fractional anisotropy and other indices of cerebral health in normal aging: tract-based spatial statistics study of aging. Neuroimage 35(2):478–487, PMID: 17292629, https://doi.org/10.1016/j.neuroimage.2006.12.021.
93. Budde MD, Janes L, Gold E, Turtzo LC, Frank JA. 2011. The contribution of gliosis to diffusion tensor anisotropy and tractography following traumatic brain injury: validation in the rat using Fourier analysis of stained tissue sections. Brain 134(pt 8):2248–2260, PMID: 21764818, https://doi.org/10.1093/brain/awr161.
94. Alba-Ferrara LM, de Erausquin GA. 2013. What does anisotropy measure? Insights from increased and decreased anisotropy in selective fiber tracts in schizophrenia. Front Integr Neurosci 7:9, PMID: 23483798, https://doi.org/10.3389/fnint.2013.00009.
95. Gautier HOB, Evans KA, Volbracht K, James R, Sitnikov S, Lundgaard I, et al. 2015. Neuronal activity regulates remyelination via glutamate signalling to oligodendrocyte progenitors. Nat Commun 6:8518, PMID: 26439639, https://doi.org/10.1038/ncomms9518.
96. Foster AY, Bujalka H, Emery B. 2019. Axoglial interactions in myelin plasticity: evaluating the relationship between neuronal activity and oligodendrocyte dynamics. Glia 67(11):2038–2049, PMID: 31038804, https://doi.org/10.1002/glia.23629.
97. Lundgaard I, Luzhynskaya A, Stockley JH, Wang Z, Evans KA, Swire M, et al. 2013. Neuregulin and BDNF induce a switch to NMDA receptor-dependent myelination by oligodendrocytes. PLoS Biol 11(12):e1001743, PMID: 24391468, https://doi.org/10.1371/journal.pbio.1001743.
98. Panlilio JM, Aluru N, Hahn ME. 2020. Developmental neurotoxicity of the harmful algal bloom toxin domoic acid: cellular and molecular mechanisms underlying altered behavior in the zebrafish model. Environ Health Perspect 128(11):117002, PMID: 33147070, https://doi.org/10.1289/EHP6652.
99. Cook PF, Reichmuth C, Rouse AA, Libby LA, Dennison SE, Carmichael OT, et al. 2015. Algal toxin impairs sea lion memory and hippocampal connectivity, with implications for strandings. Science 350(6267):1545–1547, PMID: 26668068, https://doi.org/10.1126/science.aac5675.
100. Cook PF, Berns GS, Colegrove K, Johnson S, Gulland F. 2018. Postmortem DTI reveals altered hippocampal connectivity in wild sea lions diagnosed with chronic toxicosis from algal exposure. J Comp Neurol 526(2):216–228, PMID: 28875534, https://doi.org/10.1002/cne.24317.
101. Minatohara K, Akiyoshi M, Okuno H. 2016. Role of immediate-early genes in synaptic plasticity and neuronal ensembles underlying the memory trace. Front Mol Neurosci 8:78, PMID: 26778955, https://doi.org/10.3389/fnmol.2015.00078.
102. Duclot F, Kabbaj M. 2017. The role of early growth response 1 (EGR1) in brain plasticity and neuropsychiatric disorders. Front Behav Neurosci 11:35, PMID: 28321184, https://doi.org/10.3389/fnbeh.2017.00035.
103. Sheng M, Greenberg ME. 1990. The regulation and function of c-*fos* and other immediate early genes in the nervous system. Neuron 4(4):477–485, PMID: 1969743, https://doi.org/10.1016/0896-6273(90)90106-p.
104. Peng YG, Ramsdell JS. 1996. Brain Fos induction is a sensitive biomarker for the lowest observed neuroexcitatory effects of domoic acid. Fundam Appl Toxicol 31(2):162–168, PMID: 8789781, https://doi.org/10.1006/faat.1996.0087.
105. Peng YG, Taylor TB, Finch RE, Switzer RC, Ramsdell JS. 1994. Neuroexcitatory and neurotoxic actions of the amnesic shellfish poison, domoic acid. Neuroreport 5(8):981–985, PMID: 8061308, https://doi.org/10.1097/00001756-199404000-00032.
106. Ogawa Y, Furusawa E, Saitoh T, Sugimoto H, Omori T, Shimizu S, et al. 2018. Inhibition of astrocytic adenosine receptor A_{2A} attenuates microglial activation in a mouse model of Sandhoff disease. Neurobiol Dis 118:142–154, PMID: 30026035, https://doi.org/10.1016/j.nbd.2018.07.014.
107. Chen W, He B, Tong W, Zeng J, Zheng P. 2019. Astrocytic insulin-like growth factor-1 protects neurons against excitotoxicity. Front Cell Neurosci 13:298, PMID: 31338023, https://doi.org/10.3389/fncel.2019.00298.
108. Pekny M, Pekna M, Messing A, Steinhäuser C, Lee JM, Parpura V, et al. 2016. Astrocytes: a central element in neurological diseases. Acta Neuropathol 131(3):323–345, PMID: 26671410, https://doi.org/10.1007/s00401-015-1513-1.
109. Santello M, Toni N, Volterra A. 2019. Astrocyte function from information processing to cognition and cognitive impairment. Nat Neurosci 22(2):154–166, PMID: 30664773, https://doi.org/10.1038/s41593-018-0325-8.
110. Rose J, Brian C, Pappa A, Panayiotidis MI, Franco R. 2020. Mitochondrial metabolism in astrocytes regulates brain bioenergetics, neurotransmission and redox balance. Front Neurosci 14:536682, PMID: 33224019, https://doi.org/10.3389/fnins.2020.536682.
111. Pacholko AG, Wotton CA, Bekar LK. 2020. Astrocytes—the ultimate effectors of long-range neuromodulatory networks? Front Cell Neurosci 14:581075, PMID: 33192327, https://doi.org/10.3389/fncel.2020.581075.
112. Anderson MA, Ao Y, Sofroniew MV. 2014. Heterogeneity of reactive astrocytes. Neurosci Lett 565:23–29, PMID: 24361547, https://doi.org/10.1016/j.neulet.2013.12.030.
113. Liddelow SA, Barres BA. 2017. Reactive astrocytes: production, function, and therapeutic potential. Immunity 46(6):957–967, PMID: 28636962, https://doi.org/10.1016/j.immuni.2017.06.006.
114. Escartin C, Guillemaud O, Carrillo-de Sauvage MA. 2019. Questions and (some) answers on reactive astrocytes. Glia 67(12):2221–2247, PMID: 31429127, https://doi.org/10.1002/glia.23687.
115. Risher WC, Andrew RD, Kirov SA. 2009. Real-time passive volume responses of astrocytes to acute osmotic and ischemic stress in cortical slices and *in vivo* revealed by two-photon microscopy. Glia 57(2):207–221, PMID: 18720409, https://doi.org/10.1002/glia.20747.
116. Ananth C, Gopalakrishnakone P, Kaur C. 2003. Protective role of melatonin in domoic acid-induced neuronal damage in the hippocampus of adult rats. Hippocampus 13(3):375–387, PMID: 12722978, https://doi.org/10.1002/hipo.10090.
117. Sobotka TJ, Brown R, Quander DY, Jackson R, Smith M, Long SA, et al. 1996. Domoic acid: neurobehavioral and neurohistological effects of low-dose exposure in adult rats. Neurotoxicol Teratol 18(6):659–670, PMID: 8947943, https://doi.org/10.1016/s0892-0362(96)00120-1.
118. Pulido OM. 2008. Domoic acid toxicologic pathology: a review. Mar Drugs 6(2):180–219, PMID: 18728725, https://doi.org/10.3390/md20080010.
119. Appel NM, Rapoport SI, O'Callaghan JP. 1997. Sequelae of parenteral domoic acid administration in rats: comparison of effects on different anatomical markers in brain. Synapse 25(4):350–358, PMID: 9097394, https://doi.org/10.1002/(SICI)1098-2396(199704)25:4<350::AID-SYN6>3.0.CO;2-9.
120. Sutherland RJ, Hoesing JM, Whishaw IQ. 1990. Domoic acid, an environmental toxin, produces hippocampal damage and severe memory impairment. Neurosci Lett 120(2):221–223, PMID: 2293107, https://doi.org/10.1016/0304-3940(90)90043-9.
121. Howe ML, Barres BA. 2012. A novel role for microglia in minimizing excitotoxicity. BMC Biol 10:7, PMID: 22293401, https://doi.org/10.1186/1741-7007-10-7.
122. Kato G, Inada H, Wake H, Akiyoshi R, Miyamoto A, Eto K, et al. 2016. Microglial contact prevents excess depolarization and rescues neurons from excitotoxicity. eNeuro 3(3):ENEURO.0004-16.2016, PMID: 27390772, https://doi.org/10.1523/ENEURO.0004-16.2016.
123. Mahmoud S, Gharagozloo M, Simard C, Gris D. 2019. Astrocytes maintain glutamate homeostasis in the CNS by controlling the balance between glutamate uptake and release. Cells 8(2):184, PMID: 30791579, https://doi.org/10.3390/cells8020184.
124. Mayer AMS, Guzman M, Peksa R, Hall M, Fay MJ, Jacobson PB, et al. 2007. Differential effects of domoic acid and *E. coli* lipopolysaccharide on tumor necrosis factor-α, transforming growth factor-β1 and matrix metalloproteinase-9 release by rat neonatal microglia: evaluation of the direct activation hypothesis. Mar Drugs 5(3):113–135, PMID: 18458762, https://doi.org/10.3390/md503113.
125. Mayer AM, Hall M, Fay MJ, Lamar P, Pearson C, Prozialeck WC, et al. 2001. Effect of a short-term in vitro exposure to the marine toxin domoic acid on viability, tumor necrosis factor-alpha matrix metalloproteinase-9 and superoxide anion release by rat neonatal microglia. BMC Pharmacol 1:7, PMID: 11686853, https://doi.org/10.1186/1471-2210-1-7.
126. Miller MA, Moriarty ME, Duignan PJ, Zabka TS, Dodd E, Batac FI, et al. 2021. Clinical signs and pathology associated with domoic acid toxicosis in southern

sea otters (*Enhydra lutris nereis*). Front Mar Sci 8:585501, https://doi.org/10.3389/fmars.2021.585501.
127. Colonna M, Butovsky O. 2017. Microglia function in the central nervous system during health and neurodegeneration. Annu Rev Immunol 35:441–468, PMID: 28226226, https://doi.org/10.1146/annurev-immunol-051116-052358.
128. Liu J, Liu L, Wang X, Jiang R, Bai Q, Wang G. 2021. Microglia: a double-edged sword in intracerebral hemorrhage from basic mechanisms to clinical research. Front Immunol 12:675660, PMID: 34025674, https://doi.org/10.3389/fimmu.2021.675660.
129. Liu M, Bernhardt BC, Hong SJ, Caldairou B, Bernasconi A, Bernasconi N. 2016. The superficial white matter in temporal lobe epilepsy: a key link between structural and functional network disruptions. Brain 139(pt 9):2431–2440, PMID: 27357350, https://doi.org/10.1093/brain/aww167.
130. OEHHA (California Office of Environmental Health Hazard Assessment). 2019. Domoic acid (a marine biotoxin) in fish and shellfish. https://oehha.ca.gov/fish/general-info/domoic-acid-marine-biotoxin-fish-and-shellfish [accessed 20 May 2022].
131. Zhu Z, Qu P, Fu F, Tennenbaum N, Tatters AO, Hutchins DA. 2017. Understanding the blob bloom: warming increases toxicity and abundance of the harmful bloom diatom *Pseudo-nitzschia* in California coastal waters. Harmful Algae 67:36–43, PMID: 28755719, https://doi.org/10.1016/j.hal.2017.06.004.
132. McCabe RM, Hickey BM, Kudela RM, Lefebvre KA, Adams NG, Bill BD, et al. 2016. An unprecedented coastwide toxic algal bloom linked to anomalous ocean conditions. Geophys Res Lett 43(19):10366–10376, PMID: 27917011, https://doi.org/10.1002/2016GL070023.